Design of a High Speed Water Tunnel Force Balance & Testing of High Performance Hydrofoils for Marine Hydrokinetic Turbines

Mechanical Engineering Department

University of New Hampshire

April 25, 2012

Ryan Therrien

Spencer Roux

Ben Comtois

Advisor: Martin Wosnik

Acknowledgements

We would like to thank all of the people who helped make this project possible, in particular Professor Martin Wosnik and Ivaylo Nedyalkov. Our advisor Martin Wosnik provided guidance throughout our entire project. PhD student Ivaylo Nedyalkov was very helpful with collaborating on ideas. We would also like to thank Andrew Harmon, Professor Barry Fussell, Robert Champlain, Paul Lavoie, the Ocean Research Project directors Professor M. Robinson Swift and Professor Larry Harris, the Marine Program, and the New Hampshire Sea Grant.

Abstract

This report reviews the force balance that was designed and manufactured for the UNH Six-Inch High-Speed Water Tunnel. This report also examines the design and testing of a high performance bi-directional hydrofoil for marine hydrokinetic turbines and design of a sting with cavitation assisting capabilities for studies of super-cavitation.

The force balance can read in both lift and drag measurements simultaneously, separately, and accurately. The force balance was designed for operating conditions of an up to 12 m/s (26.84 mph) flow velocity in the test section and variance in the absolute pressure from 0.2 to 2 bar (2.9 to 29 psi). The force balance is currently equipped with force measuring devices designed to test lift loads of up to 960.8 N (216 lbf) and drag loads of up to 22.2 N (5 lbs). Calibration results revealed a lift force sensitivity of 2.32 με/N (10.30 με/lb) and a drag force sensitivity of 2.66 με/N (11.85 με/lb).

The force balance allows for the testing of hydrofoils used in marine hydrokinetic turbines which currently require pitch control for bi-directional flows. A bi-directional hydrofoil will possibly decrease the cost of hydrokinetic turbine production through negating the requirement of pitch control which increases the base cost of turbines and following maintenances. The hydrofoil was designed through the modification of the NACA 63-424 hydrofoil section. Calculations using JavaFoil revealed that at their maximum efficiencies, the original NACA 63-424 hydrofoil out performs the experimental bi-directional hydrofoil with lift to drag ratios of 67.48 to 54.32 respectively. In certain scenarios the penalty of decreased performance can be outweighed by the decrease in overall turbine cost and maintenance.

A sting was designed to study the effects of super cavitation in relation to drag reduction. The sting has assisted cavitation capabilities with two ports for ventilation and pressure measurements. It utilizes a reversible mounting system to enable upstream and downstream cavitation testing. The sting can test multiple heads using an interchangeable cap system. More data will be collected as testing continues on the sting and the high performance hydrofoils.

Measuring the characteristics of 2-D hydrofoils is critical to better understand how to efficiently use them for marine hydrokinetic applications. Through the use of this force balance the UNH High Speed Six Inch Water Tunnel will help the UNH Center for Ocean Renewable Energy expand its capabilities in performing essential research.

Table of Contents

List of Figures 2
List of Tables 3
1. Introduction & Project Motivation 4
Water Tunnel Historical Background 7
2. Force Balance Design Goals 8
3. Design Process 11
3.1 Force Measurement Devices 11
3.2 Seal Design 21
3.3 Angle of Attack Setting Design 25
3.4 Hydrofoil Mount Design 28
3.5 Tunnel Support Design 29
4. Final Force Balance Design 31
5. Bi-directional hydrofoil Design for DOE reference MHK Turbine 34
7. Design of Hydrodynamic Shapes That Utilize Cavitation to Reduce Drag 37
8. Conclusion 43
9. References 45
10. Appendix 46
A.1 Alternative Designs 46
Force measurement devices 46
Sealing 48
Angle of Attack Control 52
Angle of Attack Measurement 53
Hydrofoil Mount 54
A.2 NACA foil designations 55
A.3 Additional Images 56

List of Figures

Figure 1 – Rendering of SeaGen marine hydrokinetic turbine (Marine Current Turines, Ltd.) 4
Figure 2: Example of an object travelling inside a supercavitation bubble (Wosnik et al. 2006) 6
Figure 3: The layout of the UNH High Speed Water Tunnel (Nedyalkov, 2012) 7
Figure 4: Lift forces on a NACA 0012 hydrofoil section over the operating range of the UNH high speed water tunnel (Sheldahl and Klimas, 1981). 12
Figure 5: Drag forces on a NACA 0012 hydrofoil section over the operating range of the UNH high speed water tunnel (Sheldahl and Klimas, 1981). 12
Figure 6 - Simplified force balance model used to perform the SolidWorks® simulation static study. 15
Figure 7 - Deformation resulting from lift or drag loading 15
Figure 8 - Free body diagram of a bending section (either lift or drag) and the resulting slope constraint on the end which is free to translate 16
Figure 9 - Experimental setup of lift member loading in the lift direction 19
Figure 10: Location of the strain gages on the lift sections 20
Figure 11: Strain gages applied to the lift sections 20
Figure 12: Seal test experiment setup 23
Figure 13: Cross section view of the seal design 24
Figure 14: Asymmetrical Clamp component in force balance assembly 26
Figure 15: Support plate for connecting force balance to test section 29
Figure 16: SolidWorks Simulation analysis of the plug pushing on the support 30
Figure 17: Exploded view of assembly 31
Figure 18 - Lift force calibration 32
Figure 19 - Drag force calibration 33
Figure 20: Two dimensional profile of the NACA 63-424 hydrofoil 34
Figure 21: Bi-directional hydrofoil 2D profile view 35
Figure 22: The efficiency of the original NACA 63-424 and the Bidirectional NACA 63-424 35
Figure 23: Solidworks rendering from front view of sting in hydrofoil mount 39
Figure 24: Exploded view of sting 39
Figure 25: Sting in both upstream position (Left) and downstream position (Right) 40
Figure 26: Flow field JavaFoil simulation of the low drag bi-symmetrical hydrofoil 41
Figure 27: Ventilation and Pressure paths for sting. The blue path is for ventilation, the purple path is for pressure calculations. 42
Figure 28: Slot force balance 46
Figure 29: Fixed End Force balance 47
Figure 30: Premade Strain Gage Force Balance 48
Figure 31 - Pivot seal schematic 49
Figure 32: Solidworks model of pivot seal design. 49
Figure 33 - Pivot seal test setup 50
Figure 34 - Metal bellow seal schematic. A rubber sealing surface is shown in red to allow for changing AOA. 51
Figure 35 - U-cup seal cross section schematic. Retaining ring cross sections are shown in red. 52
Figure 36: Example of a cambered hydrofoil section 55
Figure 37: General dimensioning of a hydrofoil section 55
Figure 38 - Prototype force balance used for proof of concept 56
Figure 39 - Top view of final force balance connected to tunnel 56
Figure 40 - Front view of installed final force balance 57
Figure 41 - Force balance calibration 57

List of Tables

Table 1 - Force balance design goals....8
Table 2 - Force measurement device decision matrix....13
Table 3 -Summary of of SolidWorks® FEA results and beam theory for the lift bending members....18
Table 4 - Summary of SolidWorks® FEA results and beam theory calculations for the drag bending members....18
Table 5 - Seal design decision matrix....21
Table 6: Results of the seal tests....22
Table 7: Clamping fixture decision matrix....25
Table 8: Design matrix of possible angle of attack readers....27
Table 9: Hydrofoil mount decision matrix....28

1. Introduction & Project Motivation

With the installation of the Six-Inch High-Speed Water Tunnel in the Chase Ocean Engineering laboratory, it was proposed that a force balance be designed to gather lift and drag data for experimental hydrofoils. The first task of the proposed project was to design and build a high accuracy, research-quality force balance for the new water tunnel. The second task of the proposed project was to design and test experimental high performance hydrofoils for use on hydrokinetic turbines and to determine their cavitation limits. The third and final task was to design a method to study the use of cavitation to reduce the overall drag on submerged bodies. Hydrofoil performance and hydrodynamic drag reduction are areas of active research in the marine renewable energy, hydropower and pump industries, and are of interest to a wide range of naval applications.

Task 1 focuses on designing, building and calibrating a force balance for the UNH high speed water tunnel, which will provide a platform for testing 2-D foil sections which can be used for hydrokinetic turbine applications and for studying the flow over many other lifting surfaces for different applications. For example, for marine hydrokinetic turbine applications the ability to measure 2-D hydrofoil lift and drag performance for specific operating regimes is critical for turbine performance models, and energy yield predictions. The UNH Center for Ocean Renewable Energy (CORE) is actively engaged in research on hydrokinetic turbines and will benefit from the measurement capability provided by this force balance.

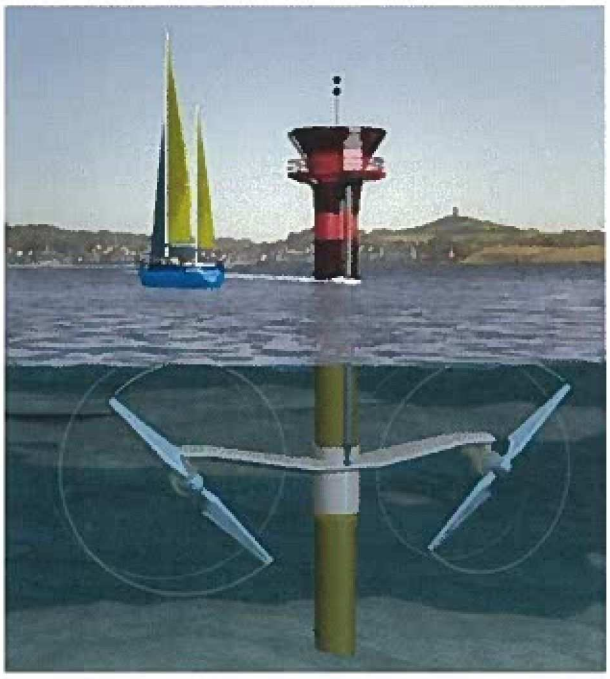

Figure 1 – Rendering of SeaGen marine hydrokinetic turbine (Marine Current Turines, Ltd.)

Task 2 focuses on the development and performance testing of a bi-directional version of the NACA 63-424 hydrofoil used on the U.S. Department of Energy (DOE) reference horizontal axis hydrokinetic turbine (RHAT) designed by the National Renewable Energy Laboratory (NREL). Investigation of a fixed angle bi-directional hydrofoil is of interest since most conventional horizontal axis tidal turbines utilize pitch control to pitch the blade in the direction of the tide which adds complexity, and considerable capital and maintenance cost. The performance of the bi-directional NACA 63-424 hydrofoil will be compared to the standard hydrofoil to make a life cycle cost vs. power production comparison. The DOE RHAT is similar in design to the 1.2MW capacity SeaGen tidal turbine located in Northern Ireland's Strangford Lough,. SeaGen, with 2x 16m diameter rotors is shown in Figure 1, and a schematic with key dimensions of the DOE RHAT is shown in Figure 2.

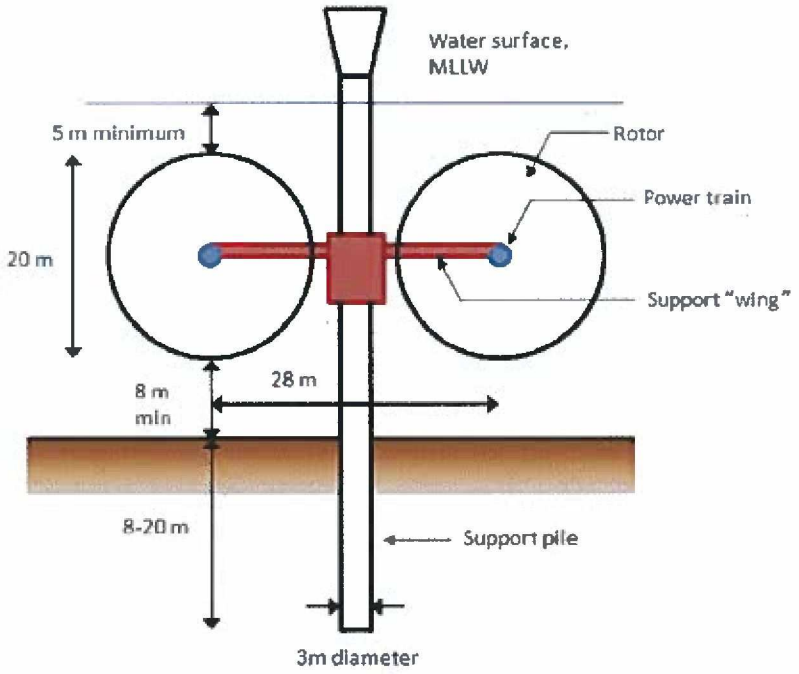

Figure 2: DOE Reference Horizontal Axis Tidal Turbine (RHAT) designed by NREL.

Task 3 focuses on the design of a platform for studying the effects of cavitation assisted drag reduction. Cavitation is a design and operating consideration for a broad variety of devices handling liquids, with examples ranging from pumps, including high-pressure fuel pumps in rocket engines, to a variety of hydro and marine turbines and marine propellers. While cavitation can have negative effects on performance, and cause noise and vibration, there is also the possibility of taking advantage of large continuous cavitation bubbles to reduce frictional drag. This has specific practical applications, e.g. using cavitation to significantly decrease the overall drag on an underwater body traveling at high speeds. To test this

phenomenon a sting was designed on which various shapes can be installed to determine their cavitation characteristics. Drag reduction is of interest both to industry for applications such as reducing the hydrodynamic drag on large ships to save fuel, and to the department of defense in reducing drag for high speed underwater vehicles and weapons. The cavitation phenomenon is explained in greater depth in Section 7. The image below shows an example of a supercavitation bubble surrounding an object moving at high speed

Figure 2: Example of an object travelling inside a supercavitation bubble (Wosnik et al. 2006)

Water Tunnel Historical Background

The original flow loop of the newly renovated UNH high-speed water tunnel located in Chase Ocean Engineering Laboratory was designed, built and tested at Saint Anthony Falls Laboratory (SAFL) at the University of Minnesota in the late 1940s and early 1950s as a 1:10 scale physical model for a 60" cavitation tunnel to be installed at the David Taylor Model Basin (DTMB) of the U.S. Department of Navy. Although the full scale 60" water tunnel was never built, the physical model was then modified and served as a 1:6 scale model for the development of a 36" variable pressure cavitation tunnel at DTMB (Straub et al 1956, Silberman et al 2009)

The current UNH high speed water tunnel schematic is shown below in Figure 3. Its test section (part #0) is 36 inches long and has inner flow dimension of six inches by six inches. There are four windows on the test section, top, bottom, and two sides. Both glass and acrylic windows can be installed on the sides of the test section depending on optical viewing requirements. Before the flow enters the test section it travels through a flow straightener (#23) to obtain a uniform flow profile and a 5^{th}-order polynomial contraction (#25) to increase the velocity of the flow. After leaving the test section the flow enters a diffuser (#1 and #2) to reduce the velocity of the flow and recover pressure. The flow is then brought back to the flow straightener (#23) through a re-circulation loop. The flow of the water is produced by a pump seen in the lower right hand portion of Figure 3. This pump can create a flow velocity in the test section of up to 12 m/s (26.8 mph). A vacuum pump attached to the section (#22) before the flow straightener is used to vary the absolute pressure from 0.2 to 2 bar (2.9 to 29 psi) in the test section.

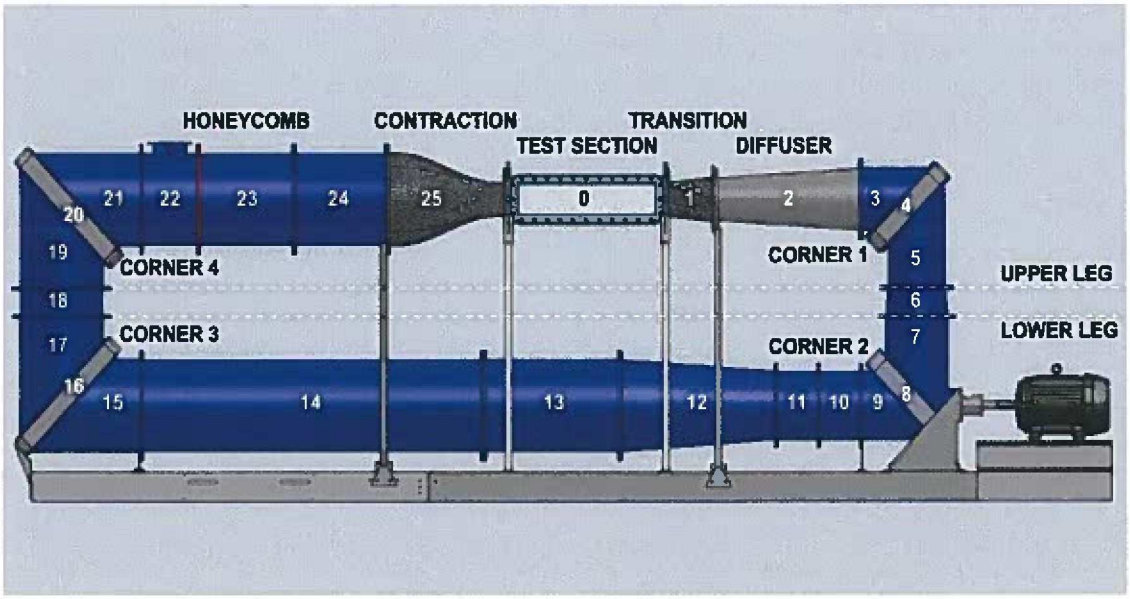

Figure 3: The layout of the UNH High Speed Water Tunnel (Nedyalkov, 2012)

2. Force Balance Design Goals

At the beginning of the force balance design, a list of design goals was created. This list is summarized below in Table 1.

Table 1 - Force balance design goals

Design Goal	Description
Simultaneous measurement of lift and drag	For conducting research on hydrofoil test sections it is advantageous to measure lift and drag simultaneously to develop a more accurate lift to drag ratio. This ensures each lift and drag measurement was taken under identical water tunnel conditions (i.e. flow speed, pressure, temperature, dissolved gas content)
Separation of lift and drag forces	Lift and drag force measurement devices should only measure forces in the lift and drag directions respectively. Since drag is much smaller than lift for a high performance hydrofoil the amount of measurement "cross talk", or lift force read in by the drag member should be kept to a minimum (and vice versa).
Minimal measurement disturbance from sealing	The water tunnel window must be penetrated and sealed, with the ability to translate in a manner that has a minimal effect on the resolution of force measurement. The restoring force of the seal will have an effect on the force measurement, but as long as it has a linear impact, this effect can be accounted for through calibration
Accuracy and repeatability of force measurement	The force balance must be accurate and take repeatable forces measurements on hydrofoil sections and cavitating shapes.
Resolution of 1N force	The measurement resolution should be at least 1N (0.22 lbf) force to quantify hydrofoil performance.
Modular design	A modular design will allow replacement or alteration of components without redesign or replacement of other separate components. Modularity should include the force measurement devices to allow for force measurement sensitivity changes based on expected range of forces. The hydrofoil mounting system must be modular so that it can accept a universal style of fixture.
User friendly design	The final design must attempt to minimize the time it takes to conduct research using the force balance, e.g. changing angle of attack.

The design of a force balance for a water tunnel is fairly unconventional and typically requires a unique design solution. The reason for constructing this force balance is to quantify hydrofoil lift and drag performance; therefore its force measurement devices must be accurate and repeatable, while recording lift and drag forces simultaneously and separately. Measuring lift and drag simultaneously is necessary to obtain the instantaneous resulting two-dimensional force for unsteady phenomena such as hydrofoil cavitation. Simultaneous lift and drag measurement ensures identical operating conditions such as tunnel pressure, temperature, and flow velocity.

Since the force balance is to be used on a water tunnel instead of a wind tunnel, there needs to be some sealing method implemented to avoid leaking where the hydrofoil mounting rod penetrates the window. Force measurement inherently requires some deflection, therefore the seal design must be allowed to translate with the hydrofoil rod, and allow the hydrofoil rod to rotate so the angle of attack can be set. The seal must perform well when subjected to pressures ranging from a vacuum of 0.2 bar (2.9 psi) absolute pressure to positive pressure of 2 bar (29 psi). The main requirement of the seal is that it must function as stated previously while having minimal effect on force measurement. Furthermore the cost, ease of manufacture, weight, efficient use of space are other goals for the design of a force measurement system.

To quantify hydrofoil performance its lift and drag must be measured over a range of angles of attack, therefore our force balance must have the ability to change angle of attack and hold it steady during an experiment. The most important goal of this portion of the design is accuracy. The angle of attack must be accurately measured relative to the flow direction and chord. To accomplish this, the instrument used to measure the angle of attack must be as accurate as possible and the device that holds the angle of attack must not fail during operation as equipment damage would be likely.

Another aspect of the design that was of importance was modularity, to be adaptable to various experiments. Since the entire force balance setup is costly, having to make large changes in the design for future experiments would further increase the overall cost of the setup. Examples of variations of possible experiments that could be performed in the water tunnel include different shapes and sizes of hydrofoil sections, changing out force measurement elements, taking surface pressure measurements, and ventilating air into the tunnel at points on an object to help induce cavitation. Therefore a modular design that allows for future experiment modifications to be made without replacing components is very desirable.

The force balance design should also be user friendly and not require too much time to change out components such as hydrofoils, the seal, or force measurement elements if needed. Ideally a person with some knowledge of its design should be able to set up and conduct experiments with the force balance. This would make it a useful piece of laboratory equipment for both graduate and undergraduate research.

3. Design Process

3.1 Force Measurement Devices

In order to select a suitable force measurement device, first we had to determine the range of lift and drag forces that the force balance would be expected to measure. A NACA foil section with readily available lift and drag coefficient data was used to determine the force measurement range for lift and drag. Here a NACA 0012 was chosen, with performance data over a wide range of Reynolds numbers and angles of attack, published by Sandia National laboratories (Sheldahl and Klimas, 1981).

To calculate the lift and drag forces acting on the foil section, first the Reynolds number, *Re*, needed to be calculated for a given water speed, with an ideal chord length of about 3.15 in using equation 1 below. The Reynolds number was found to vary from about 150,000 to 450,000 for this chord length over the operating envelope of th ehighe speed water tunnel. The closest data set for lift and drag coefficient was then chosen given this range of Reynolds numbers. Equations 2 and 3 below were used to find the lift and drag forces, F_L and F_D, that would be created on the hydrofoil in the tunnel.

$$Re = \frac{\rho V c}{\mu} \tag{1}$$

$$C_L = \frac{F_L}{\rho V^2 sc} \tag{2}$$

$$C_D = \frac{F_D}{\rho V^2 sc} \tag{3}$$

The lift and drag forces created by the NACA0012 section are shown below in Figure 4 and Figure 5 for velocities of 5, 7, 10, 12 m/s (11.2, 15.7, 22.4 and 26.8 mph). From these results the full scale lift load on a foil section with a six inch span was determined to be about 960 N (216 lbf) and the full scale drag force was determined to be about 22 N (5 lbf). Although these forces may not be the maximum lift and drag forces that could be observed during experiments performed in the water tunnel, for example during unsteady cavitation experiments, they are reasonable estimates and with an appropriate factor of safety can be used as a starting point for our measurement device design.

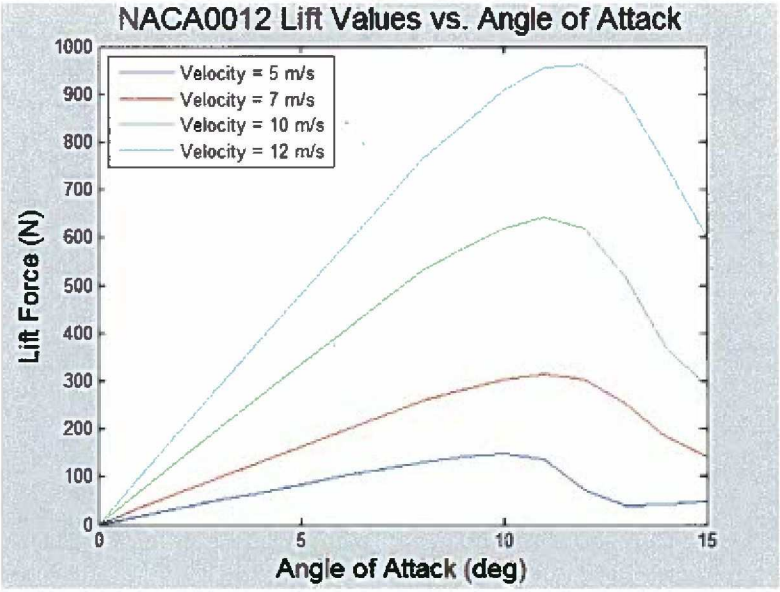

Figure 4: Lift forces on a NACA 0012 hydrofoil section over the operating range of the UNH high speed water tunnel (Sheldahl and Klimas, 1981).

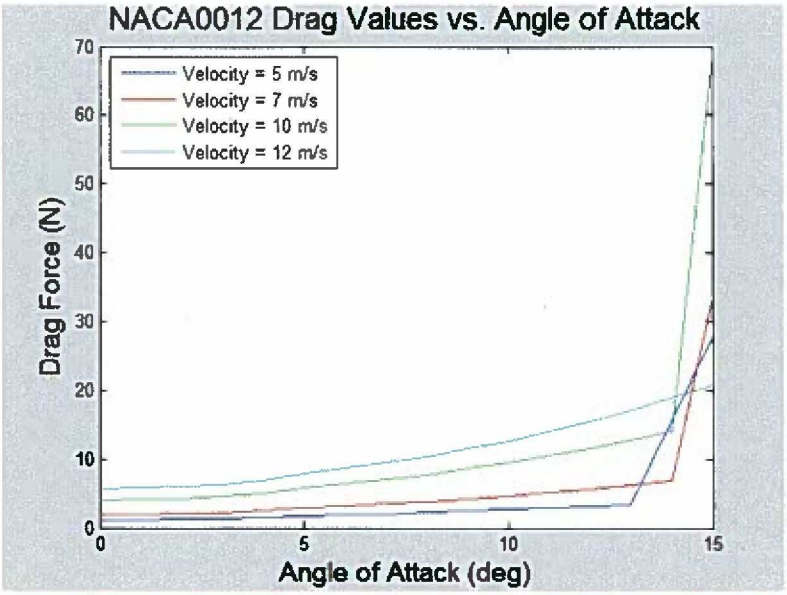

Figure 5: Drag forces on a NACA 0012 hydrofoil section over the operating range of the UNH high speed water tunnel (Sheldahl and Klimas, 1981).

Three main concepts for the force measurement devices were considered for the final force balance design and are described in the appendix of this report. To help determine the best solution for our problem a decision matrix was created rating the benefit of each design in certain categories. The design categories were also weighted to allow the more important categories to the overall design have a bigger impact in the decision process.

The most important design criteria considered was the ability to accurately separate lift and drag forces and minimize hydrofoil displacement which were both given a weight of 10. Since modularity was an overall design goal for the force balance this criteria was also given a weight of 10. Repeatability of measurements is also important, and was given a weight of 10. Complexity is important since it impacts cost, modularity, and ease of use so a weight of 8 was given to this category. Durability and ease of use were also considered important but not as much as other criteria, and were therefore given the lowest weight of 6. The following table summarizes the decision process for selecting the force measuring devices.

Table 2 - Force measurement device decision matrix

Design Criteria	Weight	Force Measurement Device		
		Bending Beam Load Cell	Tension/Compression Load Cell	Custom Bending Element
Lift and Drag Force Separation	10	8	8	10
Minimal Displacement	10	8	7	9
Durability	6	7	7	7
Repeatability	10	8	8	8
Modularity	10	1	1	10
Complexity	8	5	1	8
Ease of Use	6	5	5	8
	Total	**362**	**320**	**524**

The custom bending element with strain gages attached was found to be the clear choice. It not only meets the most important design criteria for our force balance force measuring devices, but performs better than the other options. A custom bending member can be sized specifically to resist strain in the direction it is not intended on measuring by designing it to have a high moment of inertia in that direction.

Once the force measurement design was chosen to be the custom bending elements, there were some design parameters that needed to be investigated in order to create a bending load cell that would meet the requirements. The main variables that could be chosen were the material, dimensions and the strain gages that were to be used.

The material would need to be stiff, corrosion resistant, have a high yield strength, and preferably readily available. For stiffness and availability steel is a great choice since it has a high elastic modulus and is very common. In order to obtain the necessary corrosion resistance, the material was chosen to be stainless steel. Specifically the material was chosen to be 410 stainless steel because of its high yield strength. This steel is less available and more expensive, but its stiffness and corrosion resistance fit the needs for these bending sections well.

To find required bending section dimensions in order to minimize "cross talk" and deflection while allowing adequate measurement resolution, finite element analysis (FEA) was performed in combination with beam theory calculations. The FEA was performed using SolidWorks® simulation and the beam theory analysis was used to validate the numerical results. A simplified force balance model was used for SolidWorks® simulation finite element analysis which can be seen in Figure 6.

To simplify the model all connections were bonded and bolts and bolt holes were excluded. Further simplifications included rigidly connecting the hydrofoil rod to the front plate and assuming that the support that connects the force balance to the tunnel is completely rigid and can be removed from the analysis. These complexities would significantly increase the computation time, but are only of minor importance to this analysis. Also, since we are running multiple iterations, testing different dimensions, a quicker computation time is beneficial.

Figure 6 - Simplified force balance model used to perform the SolidWorks® simulation static study.including locations of the fixtures and applied forces used for the study. Fixed geometry was applied to the end faces of the drag members and shown as green arrows. Forces were applied to the end of the hydrofoil rod shown by the blue arrows. Lift forces of 1, 320, 640, and 960 N (0.22, 72, 144, and 216 lbf) and drag forces of 1, 7, 15, and 22 N (0.22, 1.6, 3.4, and 5 lbf) were applied. Only the force in one direction was applied at a time, either lift or drag force. This allowed us to clearly see and evaluate the resolution, displacement, and "cross talk" due to these forces in each direction.

Since the bending sections are the primary focus of this analysis, a fine, high-density mesh was used for each bending section to increase the resolution of the results. A coarse, lower-density mesh was used on the hydrofoil rod and plates since they are not expected to deform significantly. The maximum deflection was measured at the end of the foil rod where

the force is applied. Results for the strain in the bending section were found at an element located in the center of the beam and 1.125 in from the back plate.

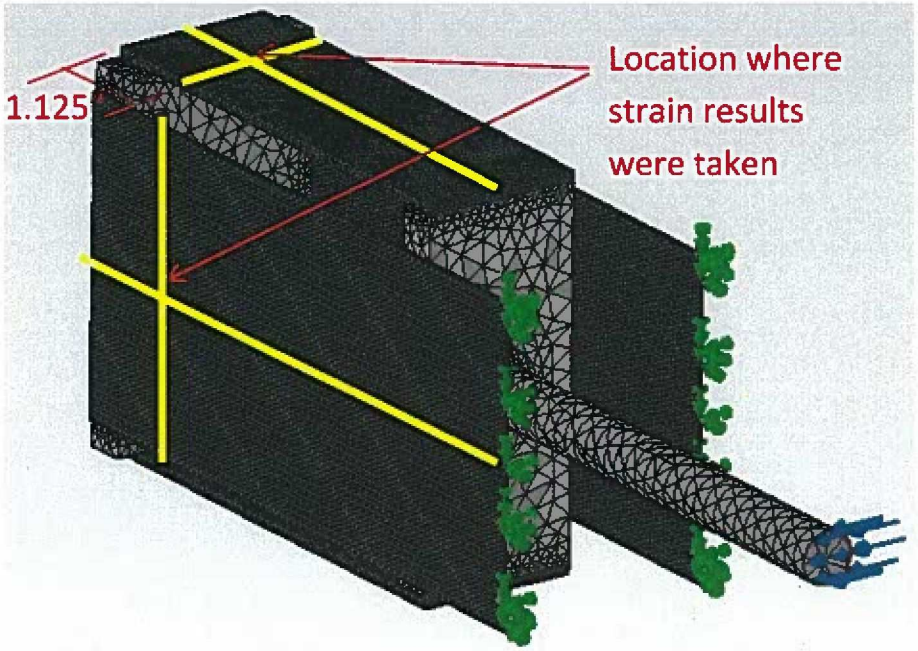

Figure 6 - Simplified force balance model used to perform the SolidWorks® simulation static study.

Figure 7 illustrates the resulting deformation from the application of either a lift or a drag force. The deformation in this figure is scaled and therefore appears much larger than it actually is. The image in the left portion of Figure 7 shows the deformation resulting from the application of a design lift force, while the figure in the right portion shows the deformation resulting from the application of a design drag force.

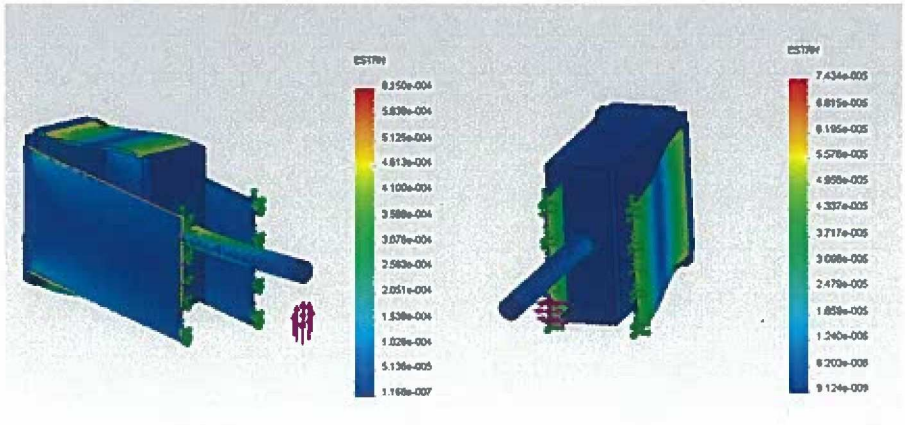

Figure 7 - Deformation resulting from lift or drag loading

After running multiple iterations, the dimensions for the bending elements were chosen from the analysis that gave the most desirable results. The lift measuring bending section dimensions were chosen to be 9.0" x 3.0" x 0.1875" and the drag measuring bending section dimensions were chosen to be 13.0" x 6.0" x 0.0625". The drag sections are made longer and thinner in an effort to increase their sensitivity. It would be ideal to increase the length and reduce the thickness of the lift sections to increase their sensitivity as well. This is not realistic though, since the lift sections will experience a much larger force and a change in dimensions to increase sensitivity would lead to too much deflection and a low factor of safety. The drag measuring sections are much wider than the lift measuring sections to increase their moment of inertia. This allows them to resist measurement "cross talk" from the relatively larger lift load.

To verify the SolidWorks® Simulation results, the problem was also solved as a statically indeterminate beam using beam theory. Figure 8 illustrates how the problem was defined in order to use beam theory. The lift members and drag members were evaluated separately to simplify the problem. Only one bending section was evaluated since they should deform nearly identically due to symmetry.

The beams were modeled as cantilevered beams with the addition of a constraint on the slope of the loaded end which must remain zero due to the fact that both lift sections and drag sections are coupled to one another. To solve the statically indeterminate problem the slope at the roller end was set to zero, and the governing equation was solved for the restraint moment. The following equations were derived.

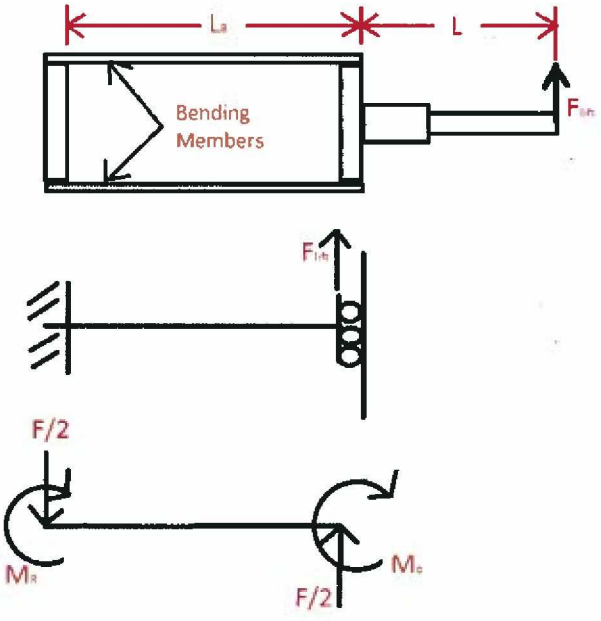

Figure 8 - Free body diagram of a bending section (either lift or drag) and the resulting slope constraint on the end which is free to translate

$$M_R = \left(\frac{F}{2}\right) L_B - M_o, \tag{4}$$

$$0 = \theta = \frac{FL_B^2}{4EI} - \frac{M_o L_B}{EI}, \tag{5}$$

Where F is the applied force, E is the modulus of elasticity. M_o is the constraint moment, I is the bending section moment of inertia, and L_B is the active length of the bending section. Solving for the constraint moment M_o yields the following equation.

$$M_o = \frac{FL_B}{4}, \tag{6}$$

Bending stress, σ_B, along the beam is then given by

$$\sigma_B = \frac{6M(x)}{Wt^2}, \tag{7}$$

Where M(x) is the moment at a given distance x along the bending section, W is the width and t is the thickness. The strain ε is then found using the stress-strain relation given by

$$\varepsilon = \frac{\sigma_B}{E}, \tag{8}$$

Similarly to SolidWorks® results, bending member strain was measured in the center of the section and 1.125 in from the back plate that joins the lift and drag members. The displacement of the bending section is given by the equation

$$\delta = \frac{FL_B^3}{3EI} - \frac{M(x)L_B^2}{2EI}, \tag{9}$$

Where I is the moment of inertia equal to

$$I = \frac{Wt^3}{12}, \tag{10}$$

Tables 3 and 4 summarize and compare the results of the SolidWorks® static study and the beam theory calculations for the lift and drag bending sections, respectively.

Table 3 -Summary of of SolidWorks® FEA results and beam theory for the lift bending members

Lift Section Analysis			
Analysis	**Load [lbs]**	**Strain [με]**	**Deflection [x 10^{-3} in]**
SolidWorks® FEA	0.25	0.6869	0.087
	72	220.0	28.2
	144	440.0	56.3
	216	659.4	84.5
Hand Calculations	0.25	0.646	0.079
	72	206.6	25.8
	144	413.2	51.6
	216	619.8	77.4
% error	0.25	5.95	8.43
	72	6.09	8.39
	144	6.09	8.38
	216	6.01	8.40

Table 4 - Summary of SolidWorks® FEA results and beam theory calculations for the drag bending members

Drag Section Analysis			
Analysis	**Load [lbs]**	**Strain [με]**	**Deflection [x 10^{-3}in]**
SolidWorks® FEA	0.25	4.87	3.56
	1.6	34.12	24.9
	3.4	73.1	53.4
	5	107.2	78.3
Hand Calculations	0.25	4.72	3.67
	1.6	33.04	25.7
	3.4	70.79	55.1
	5	103.84	82.7
% error	0.25	3.08	3.21
	1.6	3.17	3.22
	3.4	3.16	3.17
	5	3.13	5.53

From Table 3 and Table 4, it can be seen that the results of both analyses show similar trends and will be adequate confirming the dimensions of the bending sections. The required strain range for the lift member bending section is 0.466-433.9 με for a minimum load of 1 N (0.22 lbf) and maximum load of 960 N (216 lbf) of lift. The required strain range for the drag member bending sections is 1.98-45.5 με for a minimum load of 1 N (0.22 lbf) and maximum load of 22 N (5 lbf). For full scale lift loading a maximum deflection of 84.5×10^{-3} in is expected and for full scale drag loading a maximum deflection of 82.7×10^{-3} in is expected. All of these results show that the dimensions and material selections made are promising. The only result that causes concern is the small strain that needs to be measured in the lift direction in order to obtain the resolution desired.

After having chosen our material and dimensions of the bending sections, the strain gages needed to be selected. In order to select appropriate strain gages and strain gage arrangement, as well as to gather more data on this design, a physical prototype of the lift sections was designed, fabricated, and evaluated in a bench top experiment . Figure 9 - Experimental setup of lift member loading in the lift direction is shown in Figure 9.

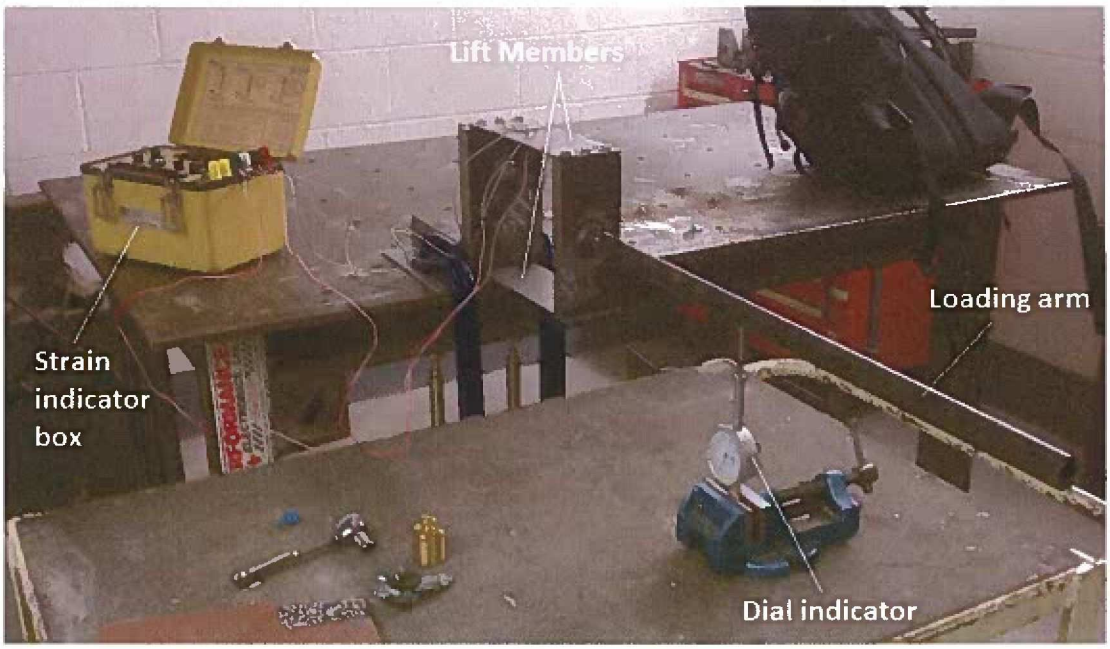

Figure 9 - Experimental setup of lift member loading in the lift direction

Two foil type strain gages were applied to the top of one of the lift sections and two were applied to the bottom of the same lift section. These strain gages had positions as shown in Figure 10 and Figure 11. The reason for only applying strain gages on one bending section and not both is because both bending sections will have nearly identical strains and the addition of extra strain gages would only increase the cost and complexity. As determined from the finite element analysis and beam theory analysis performed earlier, ideally we wanted to

use semi-conductor strain gages for the lift sections since they are able to measure smaller strains than foil type gages and therefore would yield a higher resolution. However, the foil type strain gages were readily available, so they were used for the prototype version.

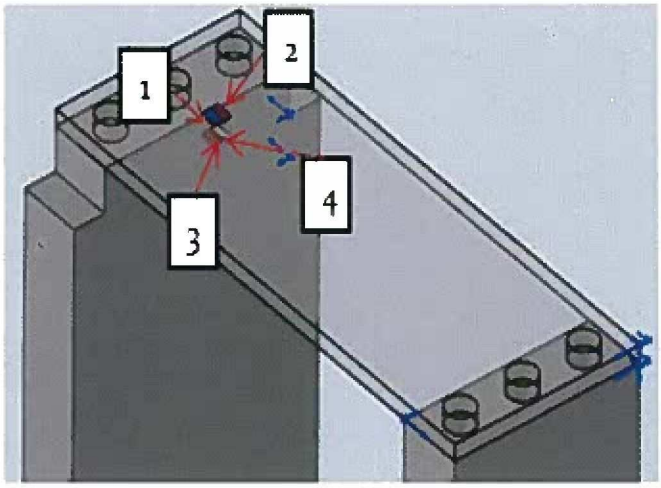

Figure 10: Location of the strain gages on the lift sections

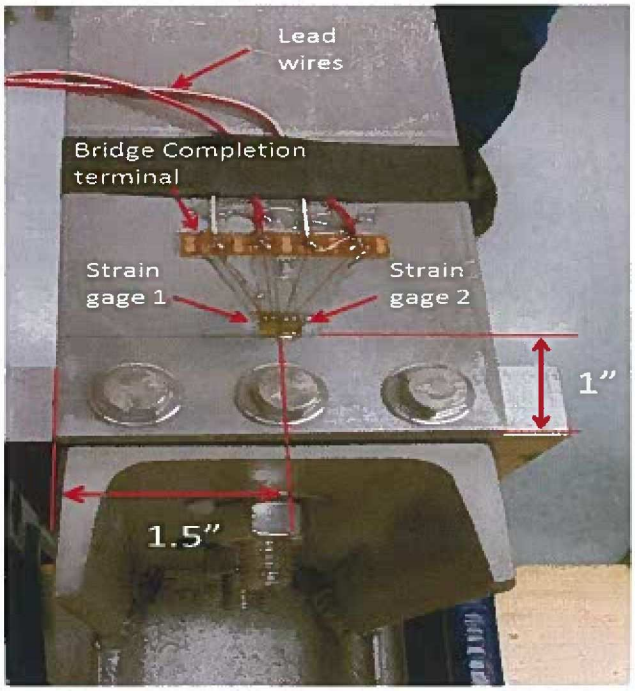

Figure 11: Strain gages applied to the lift sections

The reason there are four strain gages applied to the bending sections, also referred to as a "full bridge", as opposed to only one strain gage is that orienting and connecting them in a certain configuration can increase the sensitivity of the measurement and reduce the chance of "cross talk". After testing it was found that the sensitivity of the measurement was doubled by

using a full bridge arrangement compared to a half bridge arrangement. It was also found that the full bridge reduced the measurement sensitivity to "cross talk" by nearly four times.

3.2 Seal Design

In order to measure the forces exerted on a hydrofoil section using an externally mounted force balance, the water tunnel window must be penetrated and sealed using a suitable seal design. The seal must allow the hydrofoil rod to rotate to allow for angle of attack changes and also allow for some deflection in order for a force/strain measurement to be taken. Also, the seal must have little effect on the measurement of lift and drag forces to not decrease the resolution to an unacceptable level or introduce any non-linearity in force measurement. Similar to the force measuring devices, a decision matrix was used to help determine the best design and is shown below in Table 5.

Table 5 - Seal design decision matrix

Design Criteria	Weight	Seal Type				
		Pivot Joint	Force Balance Encasement	Metal Bellow	U-cup	Radial flex
Impact on Force Measurement	10	1	10	2	5	9
Linear Displacement	10	10	10	2	6	9
Durability	7	10	3	10	5	8
Range of Displacement	8	3	10	2	4	10
Complexity	9	1	1	10	8	8
Ease of Use	6	5	1	10	2	9
	Total	**243**	**316**	**276**	**261**	**442**

Design criteria such as force measurement impact and linearity of displacement were considered to be the most important factors and were given the highest weight factor of 10. Given the time constraints of this project and the large number of components to be designed for the force balance, complexity was given a weight factor of 9. Range of displacement, seal durability, and ease of use and were also considered important factors to allow for displacement to occur in order to obtain a measurement, maintain reliability, and be user friendly, and weights of 8, 7 and 6 were assigned, respectively.

The radial flex seal was chosen for further consideration due to its high score in the decision matrix. After choosing this design there was still a decision to be made about the material and material thickness that should be used for the final design. A testing setup was designed and manufactured in order to test the effectiveness of the trial seals. Figure 12 shows the front of the setup where the seal material was placed between the inner and outer circular clamps. In the center of the setup (not visible in this image) is a location where three O-ring grooves are used to seal the rod in the center while allowing for rotation. Also not visible in this image is the pressure tap in the back that allows for the test setup to be pressurized. Different test seals were created, placed in between the two circular clamps, and then the test setup was pressurized to 20 psi. This is about 40% higher pressure than what the tunnel is capable of and allows for a factor of safety on seals that do well in this test. If the seal could hold the pressure, the rod in the center was then moved to see the range of motion the seal had.

Table 6: Results of the seal tests

Material	Thickness (in)	Observations
Latex	0.1250	Successfully held pressure
Latex	0.0625	Bolt hole in gasket pull out
Latex	0.0500	Hole due to sharp edge
Latex	0.0400	Plastically deformed
Latex	0.0300	Plastically deformed
Latex	0.0200	Plastically deformed
Butyl (Tire Rubber)	0.0625	Not elastic enough, inconsistent properties

Figure 12: Seal test experiment setup

Results of the seal tests were recorded and are listed above in Table 6. Two materials were tested, latex and butyl rubber, but the latex had qualities that seemed to work better for this application. The latex thickness that seemed to work the best was the one eighth inch thick latex. When pressurized in the testing setup, the one eighth inch thick latex only lost one psi of pressure over nearly 48 hours.

From the results in Table 6 it is apparent that some changes to the final setup needed to be made. When the 0.050" thick latex was tested a large hole was created in the material due to a semi-sharp edge on the clamps. As a result, a radius was added to the clamps in the final design. Also, when the 0.0625" thick latex was tested the holes that were made in the material for the bolts to go through continued to be pushed out of the clamps causing leaks. Because of this a U-shaped groove was machined into the clamps in order to compress the material inwards towards the bolts and not outwards out of the clamp.

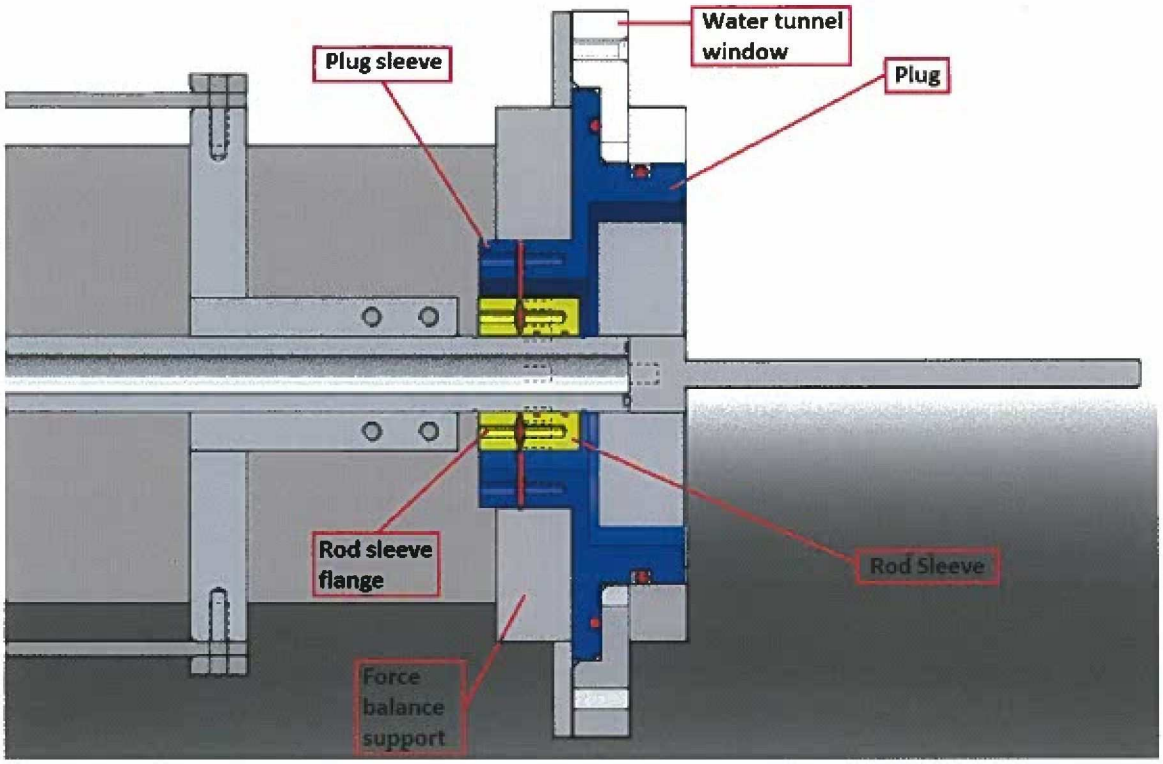

Figure 13: Cross section view of the seal design

In addition to this flexible seal for the hydrofoil rod there has to be another seal in the water tunnel window that would plug the hole needed to get the hydrofoils in the tunnel. This plug was chosen to be made out of aluminum rather than acrylic so it is easier to machine and so it could have threaded bolt holes in it for the radial flex seal. To seal this plug there are two O-rings used in between the plug and the water tunnel side window. One O-ring provides a face seal on the flange face of the plug while the other O-ring provides a radial seal. A cross section view of the final seal design is shown above in Figure 13.

3.3 Angle of Attack Setting Design

The angle of attack setting design involved two separate design criteria, one was developing a method to hold an angle of attack and the other was developing a method of measuring the angle of attack. The angle of attack setting device is a critical part of the overall force balance design since it affects the accuracy of the data taken. It is responsible for holding the hydrofoil foil arm steady at a certain angle during testing and translating all of the forces to the bending sections. The foil arm must be held completely steady, and slippage is not acceptable. There were initially six design candidates and a decision matrix was again used in order to decide a final design. Brief descriptions of the other design candidates are contained in the appendix section of this report.

Table 7: Clamping fixture decision matrix

Design Criteria	Weight	Angle of Attack Holding Designs					
		Set Screw	Gear	Gear/Clamp	Symmetrical Clamp	Asymmetrical Clamp	Collet
Ease of Assembly	3	6	3	3	8	8	2
Low Potential of Slipping	10	1	7	8	1	9	8
Size	5	5	3	4	5	5	4
Ease of Adjustment	7	7	5	5	3	7	6
Cost	5	7	2	2	5	5	2
	Total	**137**	**139**	**154**	**105**	**213**	**158**

Potential slipping is the most important criteria of angle of attack holding device because potential slipping could lead to the hydrofoil rotating to a position of very high drag and possibly damaging equipment, and therefore it has a weight of 10. Ease of adjustment is also very important since the angle of attack will most likely be adjusted several times during an experiment and therefore it was given a weight of 7. The size and costs are also significant features of each design and were both weighed at 5. The ease of assembly was the least significant feature since the force balance will be taken apart and reassembled infrequently.

The asymmetrical clamping design was chosen due to its matrix scoring and is shown below in Figure 14. This clamping design works by pushing one component against the rod creating friction between the two. The component that is pushed against the rod is oriented up stream so it cannot be unloaded due to forces created on the hydrofoil, since a negative drag force cannot occur.

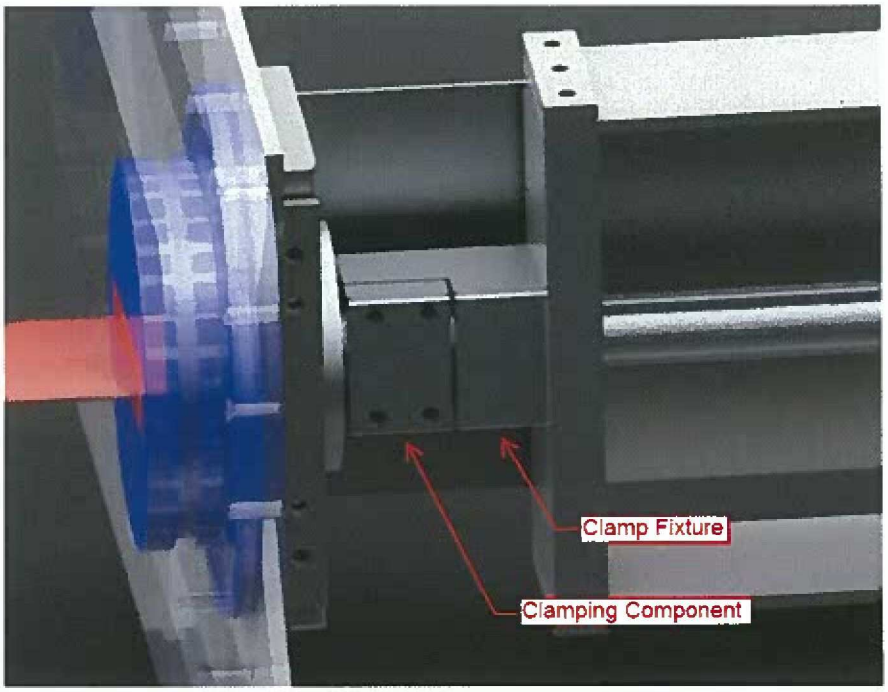

Figure 14: Asymmetrical Clamp component in force balance assembly

Once the angle of attack design was finalized, a method for measuring the angle of attack needed to be developed. Originally there were four basic designs for angle of attack measurement which are described in the appendix of this report. As with the other decisions that were made, a decision matrix was used. The accuracy of the angle of attack measuring device was the most important criteria and was therefore given a weight of 10. The size and cost of the angle measuring device are also important factors for reducing the weight, volume and cost of the force balance and were given a weight of 5. Ease of assembly would be beneficial, but is not critical and therefore was given a weight of 3.

Table 8: Design matrix of possible angle of attack readers.

Design Criteria	Weight	Angle of Attack Measurement			
		Fixed Protractor	Potentiometer	Encoder	Digital Level
Ease of Assembly	3	4	2	2	9
Size	5	4	9	9	7
Accuracy	10	5	7	8	9
Cost	5	3	7	7	9
	Total	**102**	**101**	**136**	**187**

The digital level was chosen for the final angle of attack measurement solution. Digital levels are available with varying accuracies which are reflected by their cost. A mid-range digital level with an accuracy of +/- 0.1 degrees was selected. This is an accuracy that we were originally aiming for when we began considering designs. Commonly, experiments on hydrofoils occur at angles of attack between zero and the stall angle of that hydrofoil section which is usually between 10 and 15 degrees, which means that the majority of the measurements would be taken in this range of high accuracy.

3.4 Hydrofoil Mount Design

There were three initial designs that were developed and included in the decision matrix seen below in Table 9 for the hydrofoil mount design. In this decision matrix the most weight was given to the integrity criteria, or rigidness in which the hydrofoil is held. The next highest weight was given to the versatility which is one of the main goals of the overall force balance. The cost and simplicity of the designs are also important criteria and were given a weight of 5.

Table 9: Hydrofoil mount decision matrix

Design Criteria	Weight	Hydrofoil Mount Type		
		Clamp	Bolted(Top)	Bolted(Back)
Simplicity	5	3	5	8
Versatility	6	8	5	3
Integrity	8	6	6	7
Cost	5	3	5	7
	Total	**124**	**125**	**144**

The back bolted foil mount had the highest score and was chosen for the final design. In an effort to make this design as modular as possible a rectangular insert with four ¼ -20 bolts would connect the hydrofoil and the hydrofoil rod. The universal mount has demensions 98.30mm x 25.40mm x 19.05mm (3.87"x1"x.75") which has four holes for 10-32 screws for attatching hydrofoils.

Another design consideration that is partially part of the hydrofoil mount and plug designs was a way to cover the plug of the tunnel. The large gaps between the plug walls and the hydrofoil mount would cause cavitation to occur during many operating conditions of the water tunnel. This is very undesirable since cavitation could not only affect the measurement of the lift and drag forces, but also could cause damage to equipment in the tunnel. The solution for this problem was a thin circular disk attached to the hydrofoil mount which spanned across these large gaps between the plug walls and the hydrofoil mount.

3.5 Tunnel Support Design

A support plate was designed to hold the force balance in place when an experiment is being performed. The main purpose of this support plate is to rigidly attach the force balance to the test section of the water tunnel and to secure the plug in place. To easily integrate the support plate into the current design of the test section, it was designed to use eight of the existing bolt holes that hold the water tunnel side window in place. It was also ideal to have the force balance attach only to the test section in order to keep vibrations from other water tunnel parts or experiments being performed from affecting the measurements.

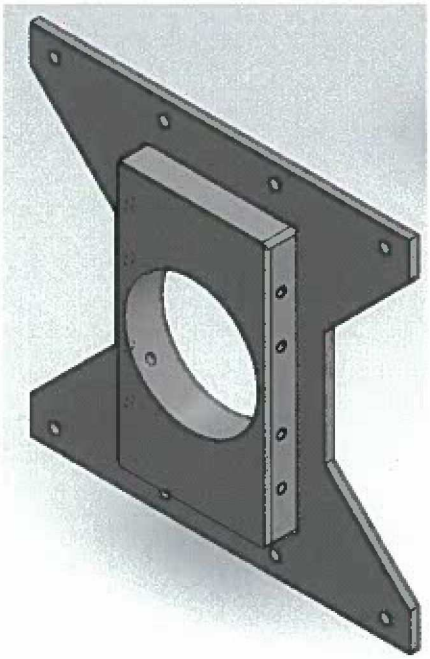

Figure 15: Support plate for connecting force balance to test section

Since the support must be very rigid and ideally not deflect at all, it was made of 410 stainless steel instead of the 6061 aluminum used for most of the other components. Steel is about three times as stiff as aluminum, depending on the exact steel and aluminum being compared and therefore steel would be better for making sure the force balance remains rigidly attached to the test section and the plug remains in place. By making the support out of stainless steel and some of the other components that come in contact with it out of aluminum, corrosion due to galvanic potential became a concern. Anti-seize paste was added to dissimilar metal surfaces to ensure that corrosion is minimized.

The support must be strong enough to keep the plug in place when the tunnel is running at its maximum operating pressure which is 2 bar (29 psi) absolute pressure. This analysis was performed assuming 15 psi which is slightly larger than the one bar pressure difference across the plug. The pressure was applied to the back face where the plug comes in contact with the

support plate. Fixed restraints were applied at the bolt holes where the support plate would be attached to the test section. A fine mesh density was used on the whole part since the computation time was small and it could lead to slightly more accurate results than a coarser mesh.

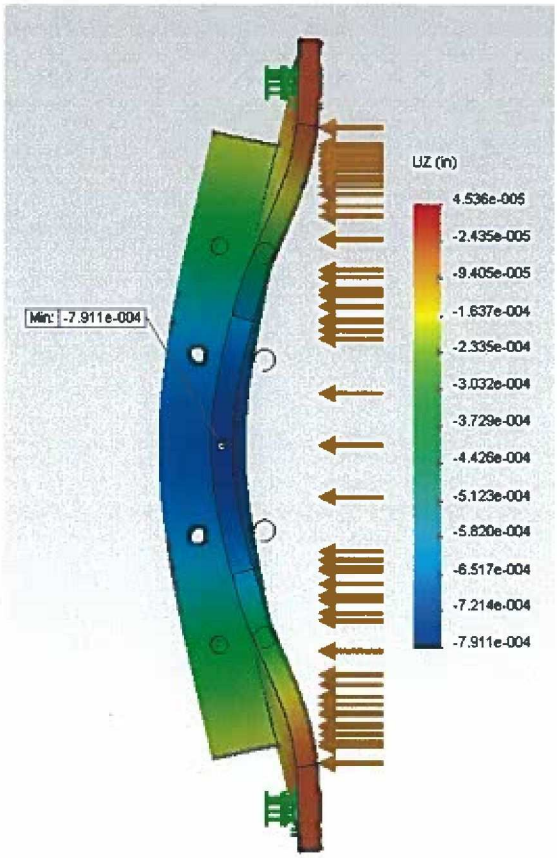

Figure 16: SolidWorks Simulation analysis of the plug pushing on the support

As can be seen from Figure 16, the pressure from the plug pushing on the support plate will slightly deform the support plate. Note that in Figure 16, the results were scaled to exaggerate the support plate deformation. The maximum deflection is located at the center of the support plate and is only 791.1 μ-in. This is acceptable and the actual deflection will likely be less than that due to the increase in stiffness from the rest of the components being attached to it.

4. Final Force Balance Design

An exploded assembly drawing of the final force balance design is shown below in Figure 17 for reference while explaining the components of the final design.

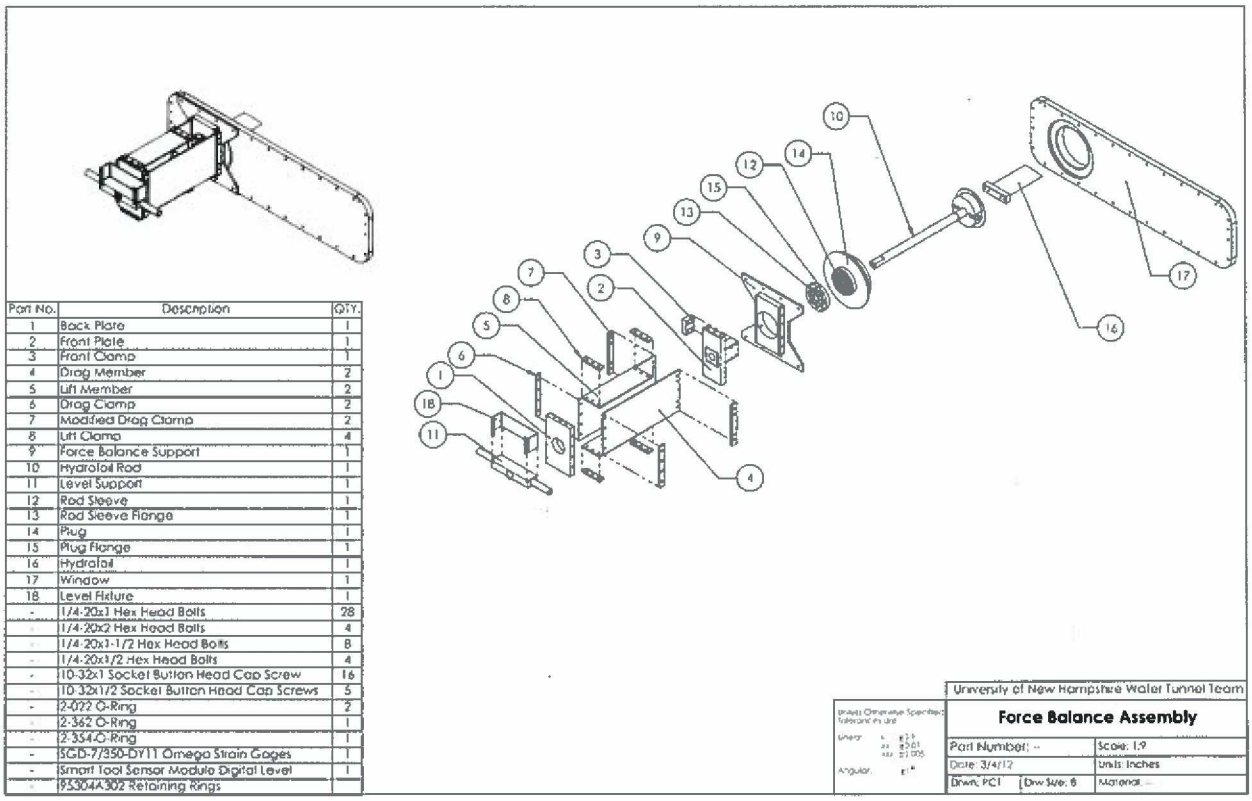

Part No.	Description	QTY.
1	Back Plate	1
2	Front Plate	1
3	Front Clamp	1
4	Drag Member	2
5	Lift Member	2
6	Drag Clamp	2
7	Modified Drag Clamp	2
8	Lift Clamp	4
9	Force Balance Support	1
10	Hydrofoil Rod	1
11	Level Support	1
12	Rod Sleeve	1
13	Rod Sleeve Flange	1
14	Plug	1
15	Plug Flange	1
16	Hydrofoil	1
17	Window	1
18	Level Fixture	1
-	1/4-20x1 Hex Head Bolts	28
-	1/4-20x2 Hex Head Bolts	4
-	1/4-20x1-1/2 Hex Head Bolts	8
-	1/4-20x1/2 Hex Head Bolts	4
-	10-32x1 Socket Button Head Cap Screw	16
-	10-32x1/2 Socket Button Head Cap Screws	5
-	2-022 O-Ring	2
-	2-362 O-Ring	1
-	2-354 O-Ring	1
-	SGD-7/350-DY11 Omega Strain Gages	1
-	Smart Tool Sensor Module Digital Level	1
-	93304A302 Retaining Rings	

University of New Hampshire Water Tunnel Team

Force Balance Assembly

Part Number: --
Scale: 1:9
Date: 3/4/12
Units: Inches
Drwn: PCT
Dwg Size: B
Material: --

Figure 17: Exploded view of assembly

Force Balance Operation:

The test hydrofoil section is mounted to the hydrofoil rod via four 10-32 screws. The hydrofoil mounting system an integral part of the hydrofoil rod was designed to accept a universal mounting block that is 98.30mm x 25.40mm x 19.05mm (3.87"x1"x.75") in the plane of the foil cross section. This allows for a hydrofoil with a maximum chord length of 3.87"/98.3mm and thickness of 1"/25.4mm. Lift and drag force is transferred from the hydrofoil through the hydrofoil mount and rod to the front plate. The force is then transferred through the lift members to the back plate which the drag members are also fixed to.

The front plate allows for the hydrofoil rod to be clamped so the angle of attack can be set for reading force measurements. Between the front plate and the foil is the water seal which has a maximum displacement of 0.25" and utilizes 1/8" thick natural latex rubber to

allow for translation of the hydrofoil rod. The force balance is fixed rigidly to the force balance support which mounts directly to the test section window. For clamping of the lift and drag bending sections, a thick clamp was used to distribute the force of the bolts and better approximate a cantilever beam condition.

The drag bending sections measure 6" by 13" and are 1/8" thick, giving them 2304 times the resistance to bending in the lift direction than in their intended force measurement direction. The lift bending sections measure 3" by 9", giving them 256 times the resistance to bending in the drag direction than in their intended force measurement direction.

Angle of attack is changed by loosening the top two bolts of the front plate AOA clamp and rotating the hydrofoil rod until the desired angle is read on the digital level which is fixed to the level support. The level support is keyed onto the hydrofoil rod via a square end, and can be fixed using a nylon set screw.

The force balance was calibrated using a range of weights applied in the lift and drag direction using a calibration tool made to simulate a hydrofoil. The calibration weight was applied at ½ the hydrofoil span of 152.4 mm (6"). The lift force and drag force calibration plots are shown below in Figure 18 and Figure 19.

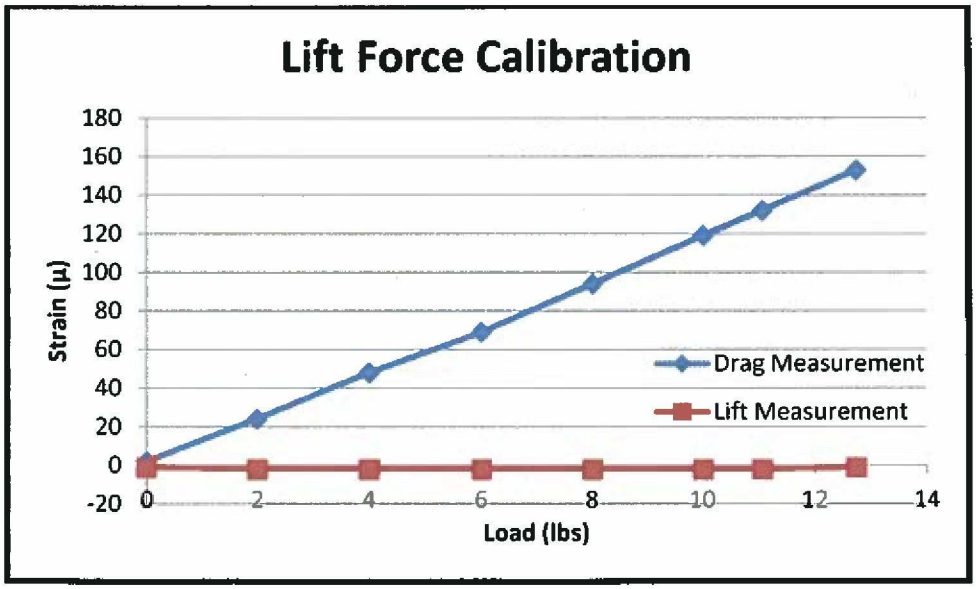

Figure 18 - Lift force calibration

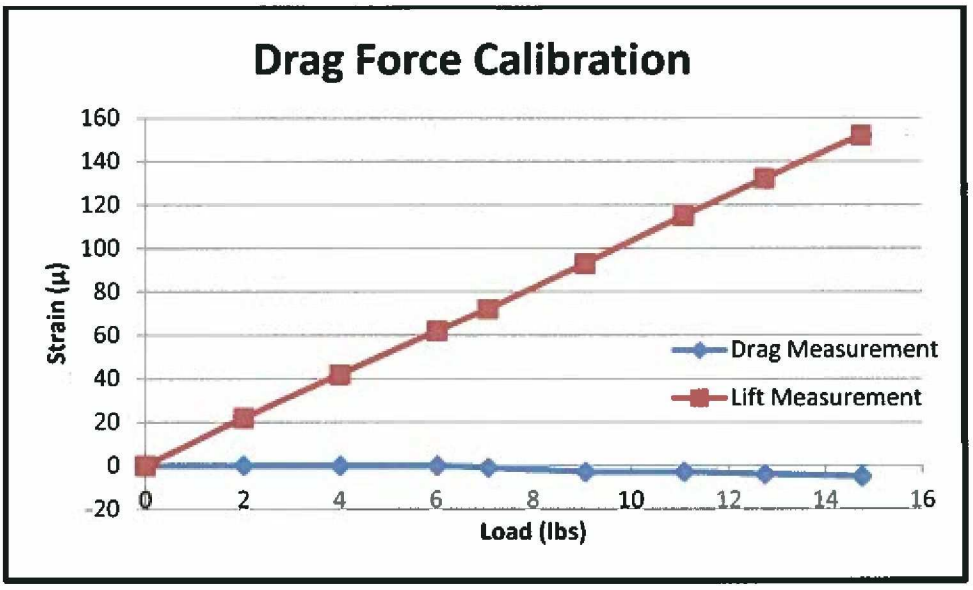

Figure 19 - Drag force calibration

Calibration results revealed a lift force sensitivity of 10.30 με/lb and a drag force sensitivity of 11.85 με/lb. This is equivalent to a lift and drag force sensitivity of 2.32 με/N and 2.66 με/N. This result shows that our resolution requirement of a 1 N (0.22 lbf) force was exceeded.

5. Bi-directional hydrofoil Design for DOE reference MHK Turbine

With the new force balance installed and calibrated, the first task was to collect data on a turbine blade hydrofoil section. The hydrofoil section that was chosen for the experiment was a NACA 63-424 hydrofoil section, seen below in Figure 20. This hydrofoil section was chosen because it makes up the outer 73% of the Department of Energy's Horizontal Axis Reference Turbine. It could be considered the most important hydrofoil section in this turbine not only because it makes up the majority of the turbine blade, but also because the majority of the power created in a horizontal axis turbine comes from the outer portion of the blade due to the higher relative velocities experienced and also the greater the torque it would create.

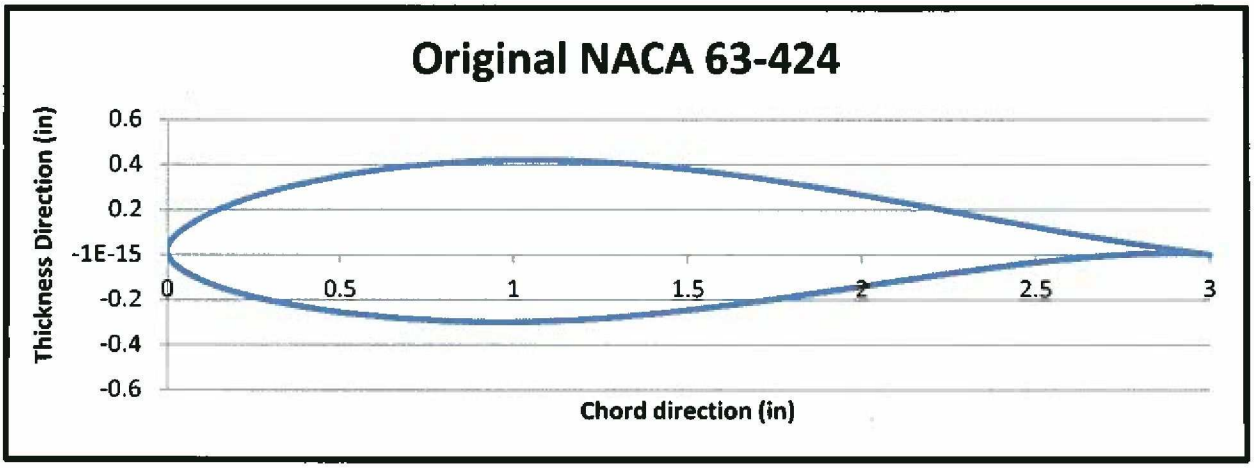

Figure 20: Two dimensional profile of the NACA 63-424 hydrofoil

The horizontal turbine that this hydrofoil section is part of is either used for single direction flow or requires pitch control to re-orient the blade for bi-directional flow. Pitch control is expensive due to extra components required for implementation and also the extra maintenance that will need to be performed. It would be beneficial to develop a hydrofoil that could be integrated into a turbine blade that would create energy from flow in both directions without having the need for pitch control.

In an effort to create this foil a modified NACA 63-424 hydrofoil section was created by mirroring the leading edge of the NACA 63-424 hydrofoil to the trailing edge and connecting these two. The two dimensional profile of this new bi-directional hydrofoil is shown below in Figure 21. This would ideally create the same lift and drag forces as the original NACA 63-424 hydrofoil section in both directions. This is not the case though, since the abrupt change at the trailing edge creates more drag on the foil and reduces the efficiency of the foil.

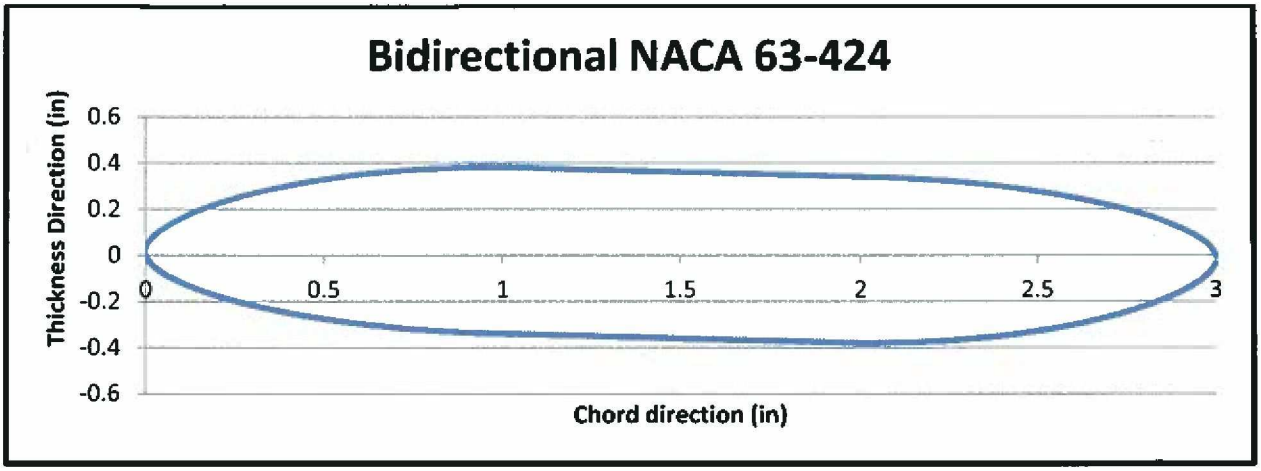

Figure 21: Bi-directional hydrofoil 2D profile view

Efficiency is normally defined as an object or system's ability to produce the desired output divided by the object or system's required input to create this output. One of the most common ways of defining the efficiency of hydrofoil sections is the ratio between the coefficient of lift and the coefficient of drag. The goal of a hydrofoil design is to produce a maximum lifting force while also having to input as little thrust possible. Figure 22: The efficiency of the original NACA 63-424 and the Bidirectional NACA 63-424 below shows the original NACA 63-424 hydrofoil section and the experimental bidirectional NACA 63-424 hydrofoil's efficiency created using calculations made in JavaFoil (Hepperle, 2008).

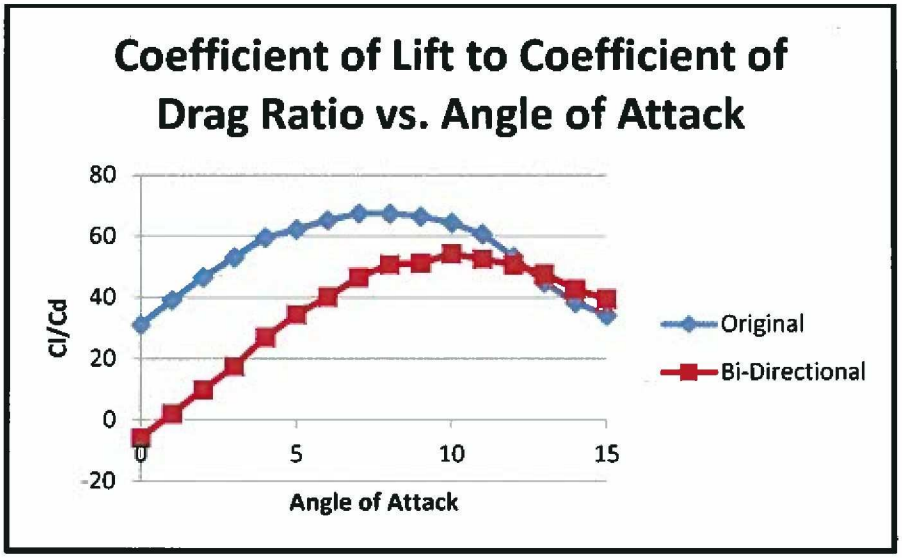

Figure 22: The efficiency of the original NACA 63-424 and the Bidirectional NACA 63-424

From reviewing these results it can be seen that the original hydrofoil section out performs the experimental bidirectional hydrofoil until an angle of attack of 13 degrees is

reached. The difference between the performances of the two hydrofoils is large at small angles of attack, but as the angle of attack increases and both of the hydrofoil's efficiencies make it to their maximum the difference between the two hydrofoils efficiently gets fairly small. The hydrofoil sections will be used in the turbine blade at the angle of attack that corresponds to their maximum efficiency. At their maximum efficiencies the original hydrofoil still out performs the experimental bi-directional hydrofoil, but the there is only about a 21.5% percent difference between them with lift to drag ratios of 67.48 to 54.32 respectively. The comparison of the cost of a pitch control system and the cost of a reduction in efficiency has to be made considering the conditions the turbine will be experiencing, but it is possible the bidirectional hydrofoil could be the ideal choice in some cases.

Another characteristic of these hydrofoils that will need to be experimented on is how they perform under cavitation prone conditions. Cavitation is the formation of cavities of steam in the flow. These cavities form when the pressure at a location in the flow drops below the vapor pressure. This causes the water of the flow to boil and form the cavity of steam. The cavitation number, shown below in equation

$$Pv0.5{\cdot}\rho v2 \quad (11),$$

which can be calculated to see if cavitation will occur at a specific location in the flow. In this equation σ is the cavitation number, P is the local pressure of the flow, P_v is the vapor pressure of the water in the flow, ρ is the density of the water in the flow, and v is the velocity of the flow at that location. If the cavitation number has a value less than one, cavitation will occur. If the cavitation number has a value greater than one, cavitation will not occur.

$$\sigma = \frac{P - P_v}{0.5 \cdot \rho v^2} \quad (12)$$

Generally the locations where these cavities are formed are at the tips of turbine blades. This is because the highest relative velocity is experienced at the tip of the blade. This is a significant problem for pumps and turbines because when these cavities collapse on the surface of the blade they can cause pitting of the blade over time. This pitting can lead to a less efficient turbine, require additional maintenance or even make the blade unusable. Gathering data on what the conditions are required for cavitation to occur will be very helpful if these hydrofoil sections are ever implemented in a horizontal axis turbine.

7. Design of Hydrodynamic Shapes That Utilize Cavitation to Reduce Drag

Cavitation occurs in water when the local water pressure falls below the vapor pressure at the given temperature causing the water to turn to vapor. This can be caused by a sharp edge which causes the flow to accelerate rapidly, and the local pressure to drop. Cavitation has practical applications because the density of water vapor is much less than liquid water. Induced cavitation can be utilized to reduce the wetted surface of an object and decrease the objects skin friction drag. At high speeds skin friction drag is the major contribution to overall drag; therefore it would be ideal to form the cavitation bubble around the entire object to reduce the wetted surface as much as possible.

Theory of drag reduction by cavitation:

The drag coefficient, C_D, can be found using the equation,

$$C_D = \frac{2D}{\rho A U^2}, \tag{13}$$

where D is the drag force, ρ is the density of water, A is the area exposed to the flow, and U is the mean velocity.

Shear stresses resulting from the flow of water on the surface area results in skin friction drag which was calculated using the equation,

$$S_f = \frac{1}{2} C_D \rho U^2 \tag{14}$$

where S_f is the skin friction, C_D being the drag coefficient, ρ being the density of water, and U being the mean water speed.

Induced drag is the drag force which comes from the trailing vortices of the entity in the flow. The induced drag coefficient can be calculated using the equation,

$$C_{Dj} = \frac{{C_L}^2}{\pi \varepsilon AR} \tag{15}$$

where C_{Dj} is the induced drag, C_L is the lift coefficient, ε is the Oswald efficiency number, AR is the aspect ratio.

The form drag is the drag due pressure at the surface of the object and can be calculated using the equation,

$$F_D = \int P \cdot \cos(\theta)\, dA \tag{16}$$

where F_D is the form drag, θ is the angle of the pressure vector, P is the pressure.

The drag force is the summation of skin friction drag, induced drag and form drag,

$$D = S_f + C_{Dj} + F_D, \tag{17}$$

where D is the net drag force, S_f is the skin friction drag, C_{Dj} is the induced drag and F_D is the form drag.

The density of steam at atmospheric pressure is .590 kg/m^3. The density of water is roughly 998.2 kg/m^3. The drag coefficient is correlated to the density. A decrease in density will result in a decrease in drag coefficient. The skin friction drag is a product of the drag coefficient, density and velocity of the flow so as the speed of the flow increases, the impact of skin friction drag increases.

Sting Design

In order to investigate super-cavitation as seen in the VA-111 Shkval torpedo, a sting was designed for the UNH 6 inch high speed water tunnel. Using cavitation to create a gas cavity for the torpedo to ride in decreases the wetted surface, reducing friction.

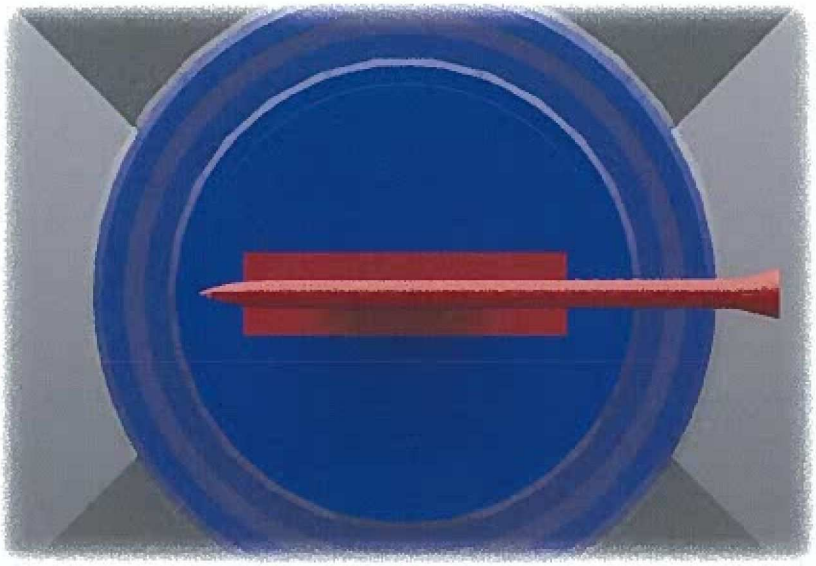

Figure 23: Solidworks rendering from front view of sting in hydrofoil mount

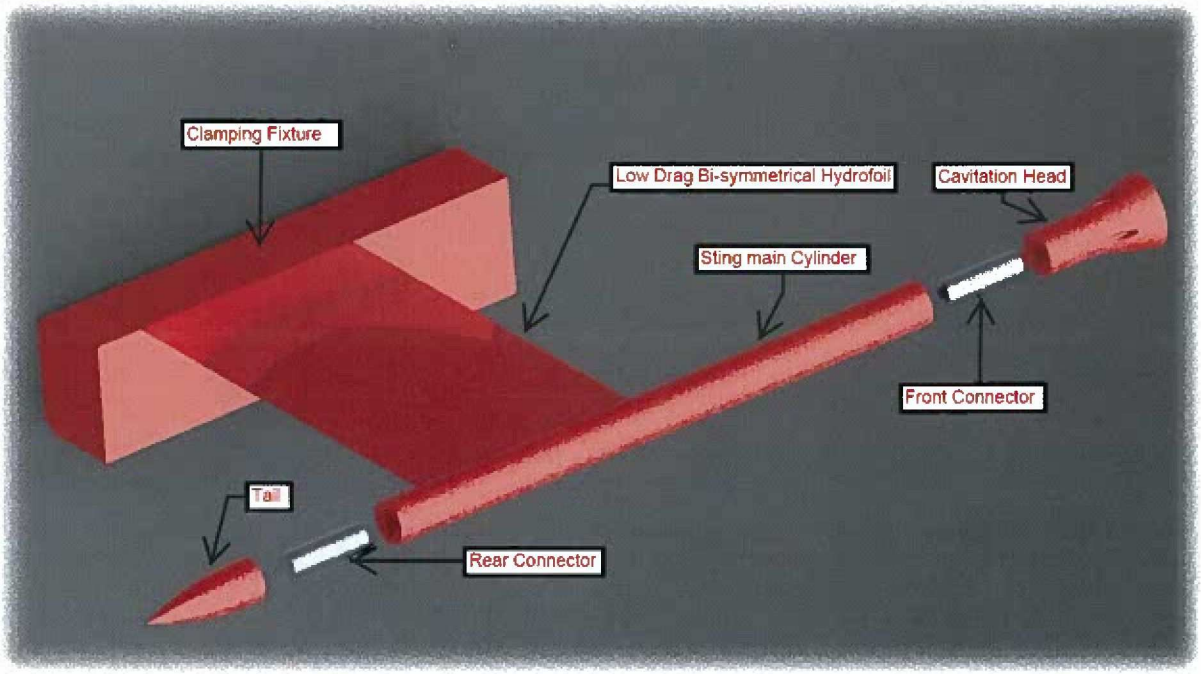

Figure 24: Exploded view of sting

The sting has 5 main design components, the clamping fixture, hydrofoil arm, main cylinder, tail end and cavitation head. In order to ensure that the minimum amount of drag will be experienced from the foil arm, a low drag bi-symmetrical hydro foil was designed. The clamping fixture fits into the existing force balance hydrofoil mount. The tail end is designed to minimize the form drag for the sting. The tail end is interchangeable to allow further testing of form drag reducing designs among other experiments. The cavitation head has been made interchangeable to enable higher versatility of the sting design, allowing for multiple tips to be tested. The intent is to make future testing easier, requiring less manufacturing.

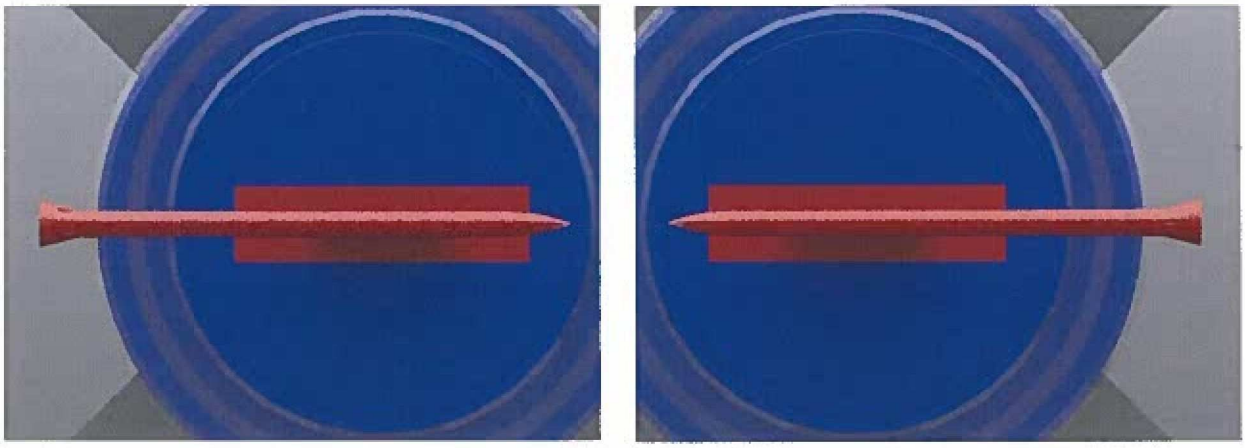

Figure 25: Sting in both upstream position (Left) and downstream position (Right)

The stings position can be reversed as seen in Figure 25. This will allow for upstream and downstream testing, using the same design. The clamping fixture portion of the hydrofoil is symmetrical which allows it to be clamped at either 0 degrees or 180 degrees.

The design of the sting went through four major iterations. For the main body of the sting, a simple cylinder design was used and a NACA 0015 foil was used originally for the arm would hold the sting cylinder in order to minimize drag. The foil is held in place using the existing hydrofoil mount, held in place using two ¼-20 bolts. In the first design the sting cylinder was connected to the hydrofoil shaft though welding. The welding has the benefit of increased strength and simplicity because no screws were needed. This design excelled in simplicity but lacked versatility.

To increase versatility of the sting the main cylinder was then going to be made reversible in the second design using two screws to attach the sting cylinder to the hydrofoil arm. In order to test multiple cavitation head designs using a single sting, a interchangeable cap system was added.

Due to testing constraints in the water tunnel, assisted ventilation would be necessary to simulate super-cavitation. In order to monitor cavitation pressure a separate vent had to be

incorporated. The earlier design incorporated the reversible sting cylinder, but complications with ventilation help and screw locations for cylinder mounting made machining of ventilation holes difficult.

In order to resolve the problem of screw and ventilation hole locations the screws were removed and the original idea of welding was investigated. The design of the clamping fixture for the hydrofoil allows for the entire foil to be placed in rotated 180 degrees. In order to deal with the significant drag that would be encountered a bi-symmetrical hydrofoil was designed.

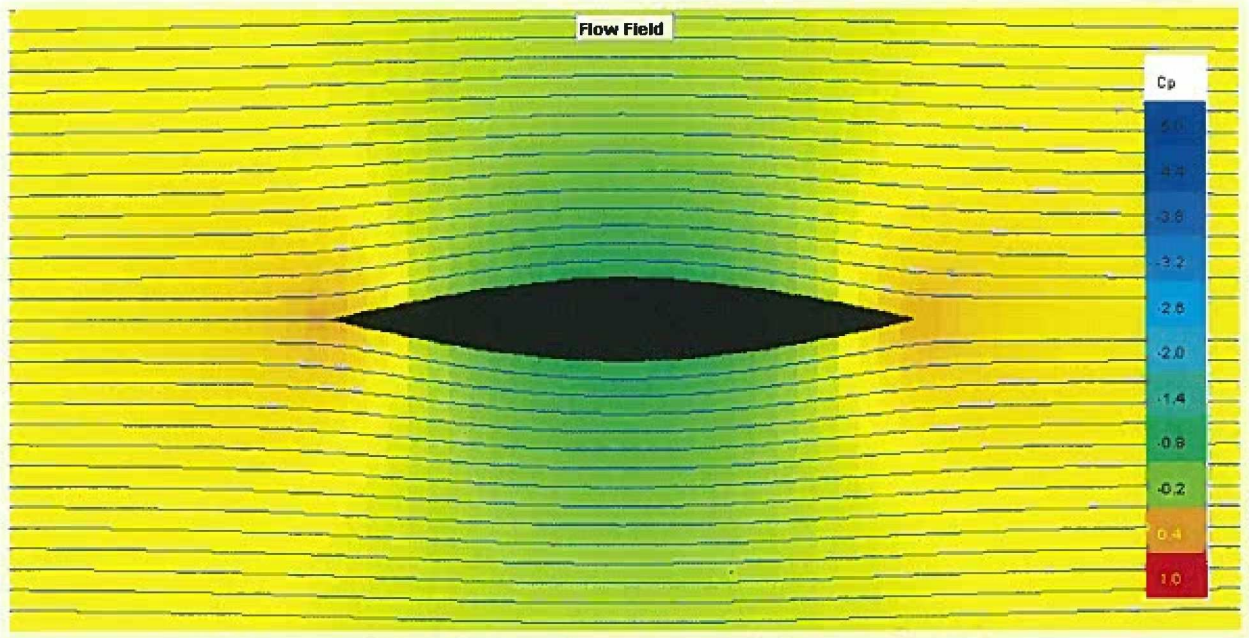

Figure 26: Flow field JavaFoil simulation of the low drag bi-symmetrical hydrofoil

The bi-symmetrical foil was created using the stream lines from the existing NACA 0021 foil. A NACA 0012 foil has a coefficient of drag of .0135. The penalty for using the new low drag bi-symmetrical hydrofoil was a coefficient of drag increase of .0001, with a total of .0136.

This design will be assisted cavitation capable. The tunnel will be running sub-atmospheric so the tubing that will be running into the sting will not require a pump. With this technique however it will require pressure readings in the gas cavity for cavitation calculations.

To measure the pressure of the gas cavity, a pitot tube and manometer set up will be used. In order to convert the manometer height readings to absolute pressure, the equation,

$$P_{absolute} = P_{atm} - (\Delta d - d_{ref}) * \rho_{water} * g, \quad (18)$$

will be used where $P_{absolute}$ is the absolute pressure which is calculated using atmospheric pressure,P_{atm}, change in manometer height, Δd, reference height , d_{ref}, density of water, ρ_{water}, and gravity, g.

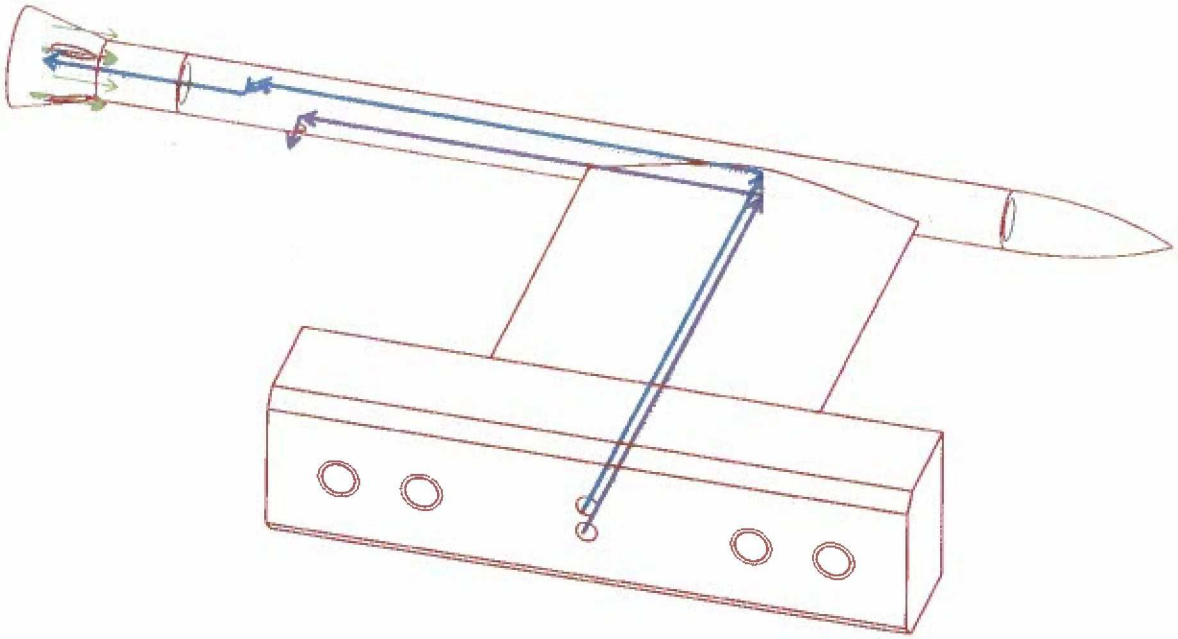

Figure 27: Ventilation and Pressure paths for sting. The blue path is for ventilation, the purple path is for pressure calculations.

The sting is in the process of being quoted and will be manufactured. In order to test the design the pieces have been rapid prototyped for pre-testing. Due to the rough surface finish from rapid prototyping, filler and sanding will be needed.

8. Conclusion

The force balance was designed to provide a platform for testing 2-D foil sections which can be used not only for hydrokinetic turbine applications but also for studying the flow over many other lifting surfaces for different applications. This report reviews the force balance that was designed and manufactured for the UNH Six-Inch High-Speed Water Tunnel. This report also examines the design and testing of a high performance bi-directional hydrofoil for marine hydrokinetic turbine use. Lastly, this report explores the design of a sting with cavitation assisting capabilities for studies of super-cavitation.

The force balance was designed for operating conditions of up to 12 m/s (26.84 mph) flow velocity in the test section and variance in the absolute pressure from 0.2 to 2 bar (2.9 to 29 psi). The hydrofoil mounting system of the force balance can accept a universal mounting block that is 98.30mm x 25.40mm x 19.05mm (3.87"x1"x.75"). This allows for a hydrofoil with a maximum chord length of 98.3mm (3.87") and thickness of 25.4mm (1").

The force balance can read in both lift and drag measurements separately and simultaneously with accuracies in angle of attack readings within ± 0.1 degree. The force measuring devices of the force balance are customizable for varying operating loads and sensitivities. The force balance is currently equipped with force measuring devices designed to test lift loads of up to 960.8 N (216 lbf) and drag loads of up to 22.2 N (5 lbf). Calibration results revealed a lift force sensitivity of 2.32 με/N (10.30 με/lbf) and a drag force sensitivity of 2.66 με/N (11.85 με/lbf).

The force balance allows for the testing of hydrofoils used in marine hydrokinetic turbines which currently require pitch control for bi-directional flows. The components required for pitch control increase the cost of turbines and maintenance. The bi-directional hydrofoil does not require pitch control for bi-directional flows. The hydrofoil was designed through the modification of the NACA 63-424 hydrofoil section, mirroring the leading edge to the trailing edge.

From the theoretical JavaFoil simulations it was seen that the original NACA 63-424 hydrofoil section out performs the experimental bi-directional hydrofoil until an angle of attack of 13 degrees is reached. At their maximum efficiencies the original NACA 63-424 hydrofoil out performs the experimental bi-directional hydrofoil, with lift to drag ratios of 67.48 to 54.32 respectively. In certain scenarios the penalty of decreased performance can be outweighed by the decrease in overall turbine cost and maintenance. These bi-directional hydrofoils can also be used in a variety of other situations, such as bi-directional thrusters for marine applications.

A sting was designed to study the effects of super cavitation in relation to drag reduction. The sting has assisted cavitation capabilities with two ports for ventilation and

pressure measurements. It utilizes a reversible mounting system to enable upstream and downstream cavitation testing. The sting can test multiple heads using an interchangeable cap system. More data will be collected as testing continues on the sting and the high performance hydrofoils.

For marine hydrokinetic turbine applications the ability to quantify 2-D hydrofoil lift and drag performance for specific operating regimes is critical and the UNH Center for Ocean Renewable Energy will benefit from this capability provided by the high speed water tunnel force balance.

9. References

Beer, David F., and David A. McMurrey. *A Guide to Writing as an Engineer*. Hoboken, NJ: Wiley, 2009. Print.

Beer, Ferdinand P. *Mechanics of Materials*. 5th ed. New York: McGraw-Hill Higher Education, 2009. Print.

"NACA Airfoil." *Wikipedia*. Web. 2011. <http://en.wikipedia.org/wiki/NACA_airfoil>

Nedyalkov, I. Section and Diffuser for a High-Speed Water Tunnel.

Sheldahl, R. E. and P. C. Klimas. *Aerodynamic Characteristics of Seven Airfoil Sections*. Sandia National Laboratories, Albuquerque, NM. 1981.

Silberman E; Arndt REA; Wosnik M (2009) The life and times of the six inch tunnel. *The Channel* - St Anthony Falls Newsletter, Fall 2009.

Straub LG; Ripken JF; Reuben RM (1956) The Six-Inch Water Tunnel at the St. Anthony and Its Experimental Use in Cavitation Design Studies, Technical Paper No. 16, Series B, St Anthony Falls Laboratory, University of Minnesota.

Hepperle, M. JavaFoil, 2008. <http://www.mh-aerotools.de/airfoils/javafoil.htm>

10.Appendix

A.1 Alternative Designs

Force measurement devices

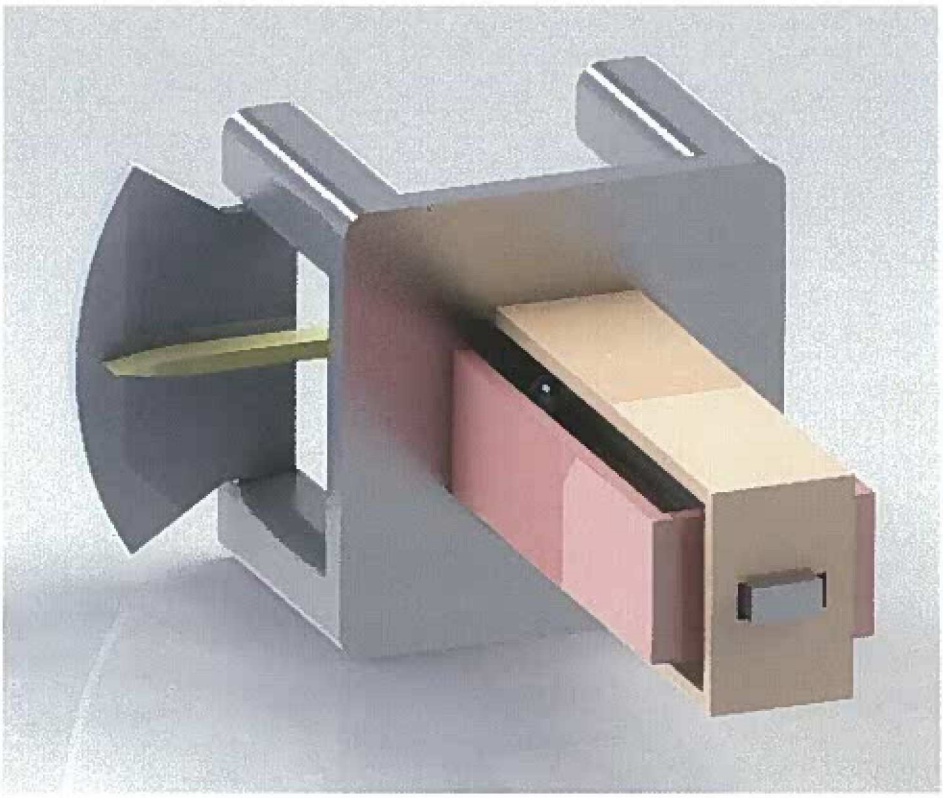

Figure 28: Slot force balance

Figure 28 is seen above and operates using two bending sections shown in orange and red. The orange is oriented to read in lift data, the red is oriented to read in drag data. Force measurements would be recorded with strain gages applied to high stress locations on the face of the bending members. The two bending sections are not attached to one another and function from deflections in the bar. The slots cut from the orang bending section seen on the front allows the bar to shift horizontally(drag) while accepting forces vertically(lift). This theoretically would separate the lift and drag measurements. The same design was applied for the red bending section, with a slot cut to allow for translation in the lift direction while accepting forces from the drag.

In order for this design to work it would need to operate on a hinge, which would be seated in the base plate (the semi-square section at the base of the bending sections). A clamp

would be attached at the base with the angle of attack measured in using a fixed needle with protractor to read in the angle.

The advantages of this design is the complete theoretical separation of lift and drag measurements. In application however the reaction of the torque is unknown.

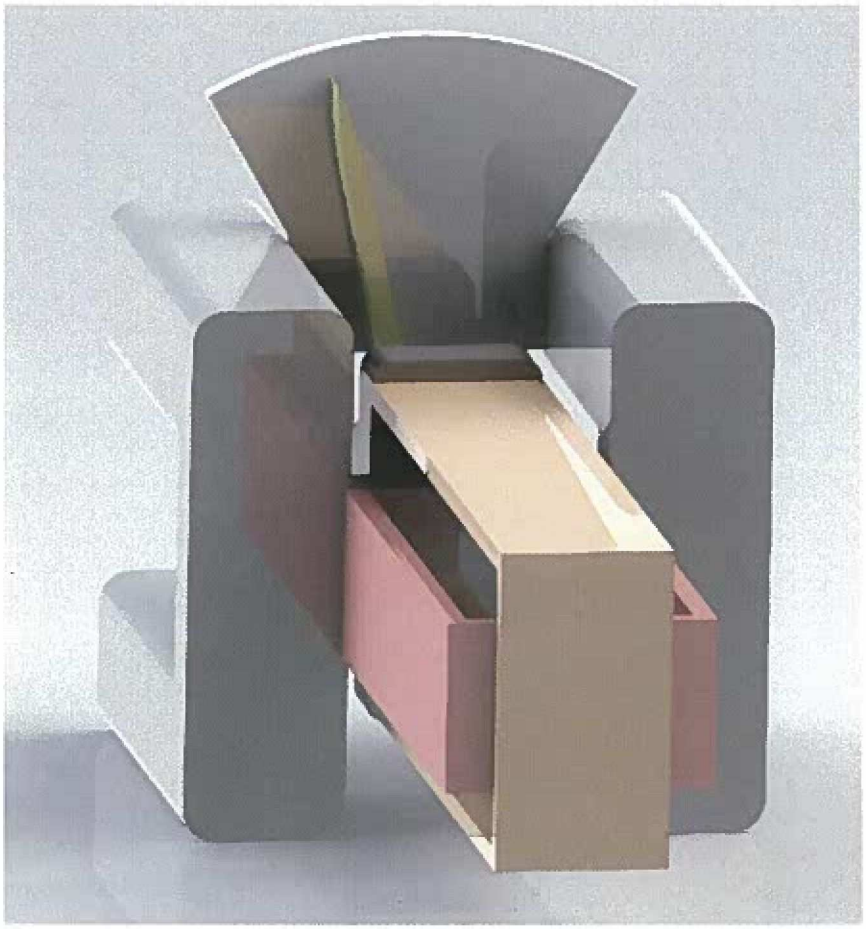

Figure 29: Fixed End Force balance

Figure 26 operates using two bending sections shown in orange and red. The orange is oriented to read in lift data, the red is oriented to read in drag data. Force measurements would be recorded with strain gages applied to high stress locations on the face of the bending members. The two bending sections are rigidly attached with each other. This design was chosen for further consideration and was the basis to our final design.

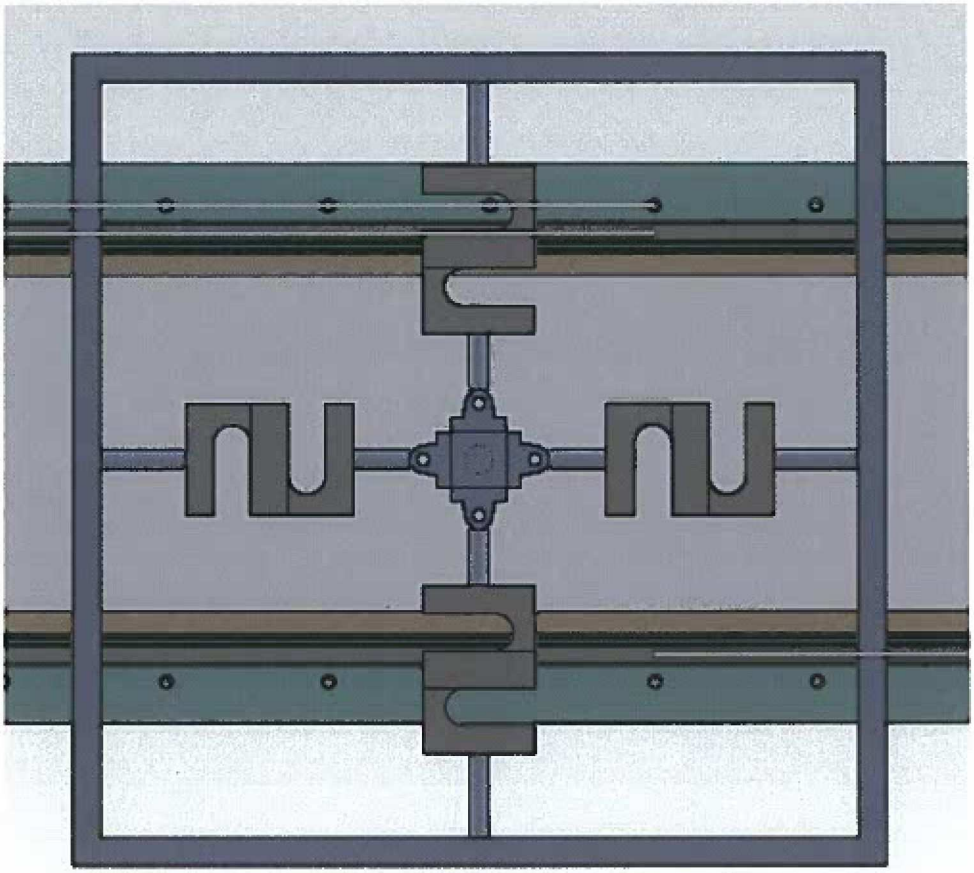

Figure 30: Premade Strain Gage Force Balance

Figure 27 shows the set up for the Premade Strain Gage Force Balance. The force balance would operate using 4 bending type load cells acting on a set of rails. The load cells oriented vertically would measure lift while the horizontal load cells would read in drag.

The rails would fix the lift cells in the y direction and the fix the drag cells in the x direction. The forces from the moment around the hydrofoils could be calculated using this design through the differences in force measurement between the adjacent load cells. This design was ruled out due to complexity of testing and anticipated high cost of manufacturing.

Sealing

Pivot Joint Seal

The first seal design investigated beyond the initial conceptual idea was a pivot joint enclosed in the water tunnel window. This idea was thought to have the ability to seal the tunnel and provide a way of selecting the magnitude of the lift and drag force being measured based on the selection of the length L shown below in Figure 31.

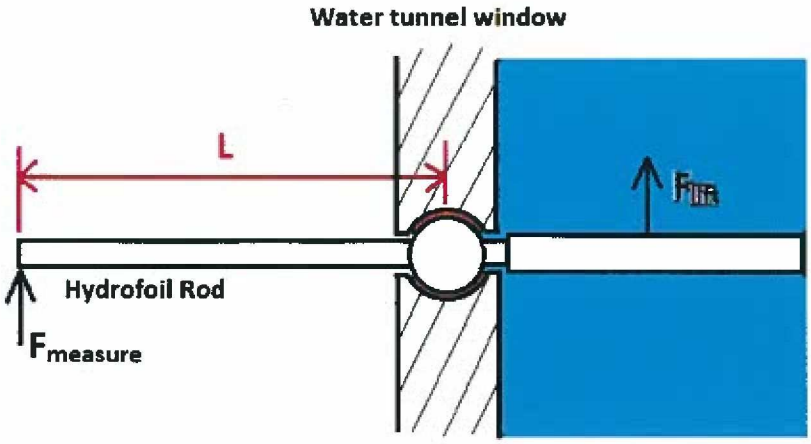

Figure 31 - Pivot seal schematic

The figure below is an isometric view of the pivot seal design.

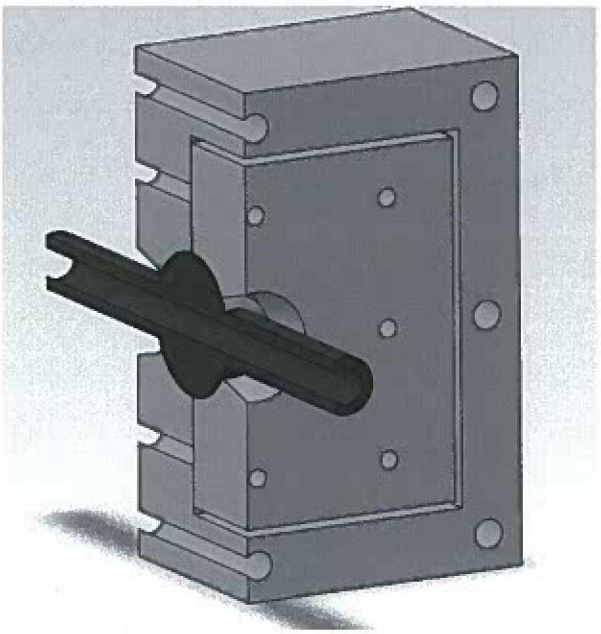

Figure 32: Solidworks model of pivot seal design.

In order to read in pressure measurements inside the hydrofoils, inside the tunnel, the tube traveling through the pivot seal had to be hallowed. The circular pivot point would be compressed in between two square sections to seal the water tunnel.

Paul Lavoie, a Research Project Engineer for the Chase Ocean Engineering Laboratory let us borrow a prototype pivot seal he had made for a previous project to perform some tests to validate the ability of the pivot ball to seal with minimal rotational friction. This was

accomplished by creating a flange and gasket to seal off one side of the pivot for pressure testing. Figure 33 below shows the experimental setup.

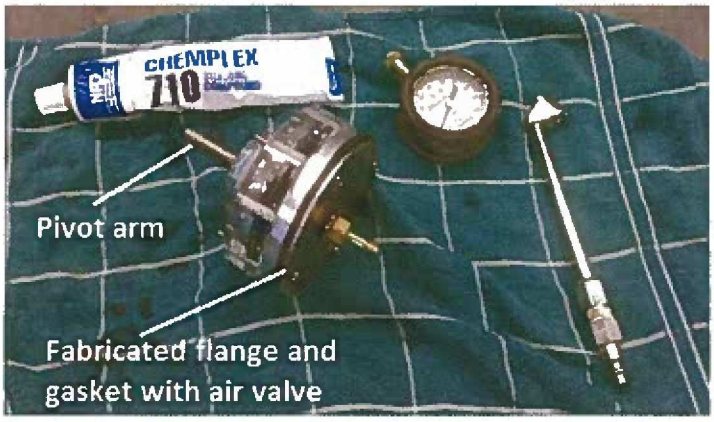

Figure 33 - Pivot seal test setup

Testing of the pivot seal was done by pressurizing it to 20 psi at which point the handmade butyl rubber gasket blew out. The pressure was then reduced to 10 psi where blowout did not occur, but leakage around the pivot ball was observed using a soap and water mix. At 10 psi the amount of rotational friction between the pivot ball, and delrin plastic sealing surface was very large despite the use of silicon grease, limiting the movement of the pivot arm considerably. For this reason it was decided that pursuing this idea further might be costly and very time consuming, therefore other more simple solutions were investigated.

Force Balance Encasement

The most basic idea for a sealing solution was to encase the force balance in a water tight box with holes only for outgoing strain gage or load cell wires. This solution would eliminate the impact of sealing on force measurement, but introduce other concerns such as material corrosion, encasement failure at high water tunnel pressures, and lack of usability. This idea was considered impractical for changing angle of attack or switching hydrofoils and therefore was abandoned.

Metal Bellow Seal

An off the shelf seal called a metal bellow seal was also considered. The metal bellow seal can allow a small amount of deflection via a flexible metal bellow shaped section while still maintaining the ability to rotate, allowing the angle of attack to be changed. The metal bellow seal schematic is shown below in Figure 34.

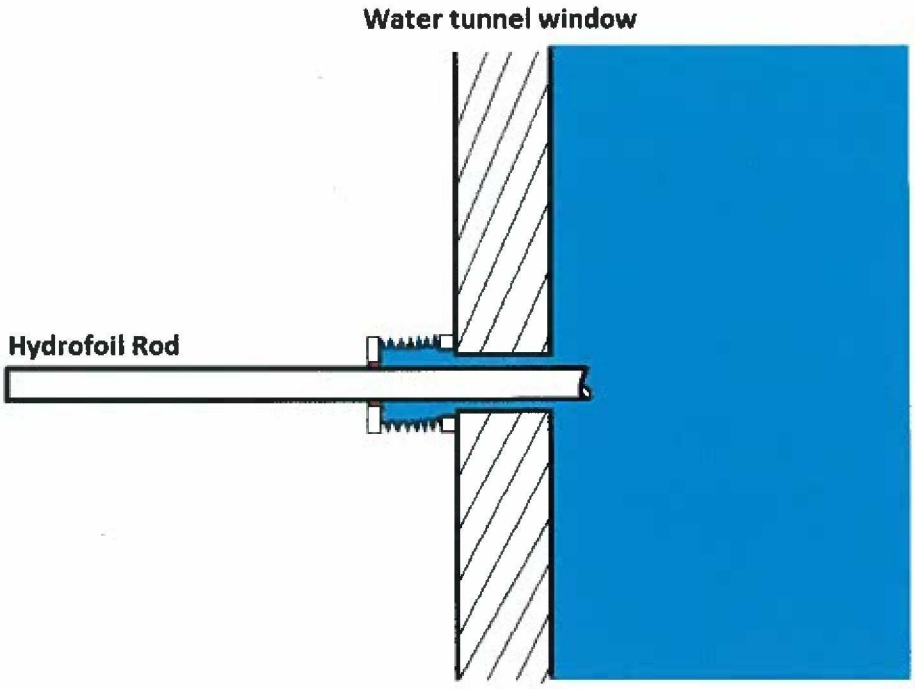

Figure 34 - Metal bellow seal schematic. A rubber sealing surface is shown in red to allow for changing AOA.

Despite contacting manufacturers directly it was difficult to obtain specific data regarding the deflection characteristics for a metal bellow seal. Due to lack of published information, or time to test the deflection of a bellow seal ourselves, it was ultimately determined not suitable for our application.

Rubber U-cup Seal

Another off the shelf seal Idea that was investigated was the use of a rubber U-cup seal fitted to the diameter of the hydrofoil rod. It was thought that two U-cup seals back to back as shown in the schematic below would be self-sealing based on a pressure differential.

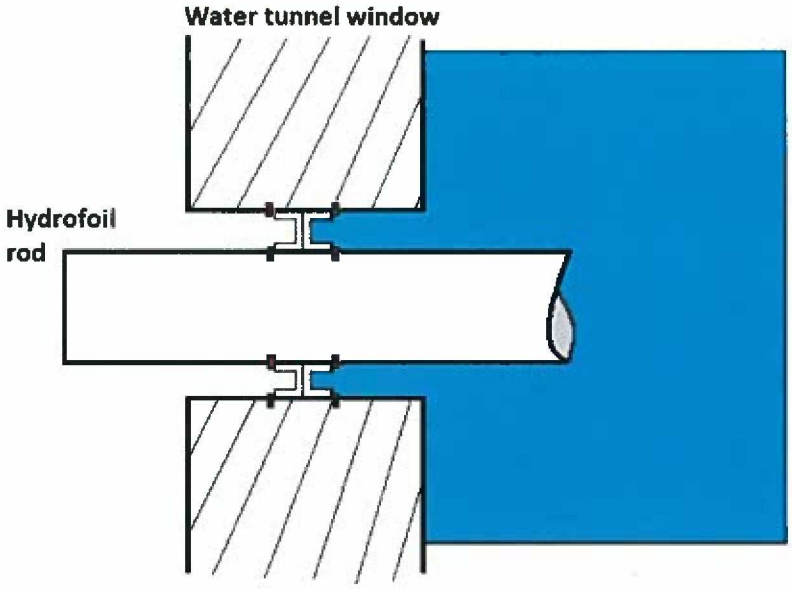

Figure 35 - U-cup seal cross section schematic. Retaining ring cross sections are shown in red.

Figure 35 illustrates the use of two U-cup seals oriented back to back and held in place with two external retaining rings on the hydrofoil rod, and two internal retaining rings on the water tunnel window. A pressure differential across the seal was thought to increase the ability of the seal to prevent water leakage or air intrusion in the case of a sub atmospheric water tunnel pressure. Hydrofoil rotation would be possible using silicon grease applied to the U-cup contact surfaces to aid in sealing and rotation. It was attempted to validate the ability of the seal to function as well as deflect using PVC pipe in a very similar setup as shown in Figure 35. It was found that PVC was a poor choice of test material despite its lower cost. Issues of roundness were encountered when machining, ultimately destroying the test apparatus. It was determined that a metal prototype would need to be made to validate the design, and that given the expense and confidence in the design, it was not worth the gamble to pursue further.

Angle of Attack Control

Set Screw Design: A set screw design would fix the angle using a simple set screw holding the bar at a fixed angle of attack. Advantage of this is the quick and easy to set of angle of attack, low cost and ease of assembly. However the pin does not provide great clamping strength and may be susceptible to slipping. Repeated tightening of the set screw would also cause damage to the face of the bar.

Gear Fixture Design: This design would be composed of gearing attached to the foil arm. A rotating handle would have a fixed gear ratio. Every rotation of the arm would result in a

change in angle of attack by some set degree. The angle of attack would be fixed through locking the gears with a key. By having an indicator of the angle of attack geared in, this design would act as both the angle of attack control and measurement. A gear fixture design would have an advantage of being easy to set but the design was bulky requiring multiple custom parts with a complicated assembly.

Gear and Clamping Combination: Similar to the gear fixture design, the angle of attack could be controlled via a set of gears. The angle would be locked in place using a clamp on the foil arm rather than locking the gears. The gear and clamping combination design had good strength potential but seemed too intricate and overcomplicated what should be a simple component.

Symmetrical Clamp Design: A simple clamp would fix the foil arm. Adjusting the foil arm would be done directly without added gearing components. An arm fixed directly to the foil arm could be used to modify the angle of attack after the clamp had been loosened. The symmetrical clamp design weak points were during angle of attack adjustment periods the tunnel seal would be responsible for holding up all the weight of the foil and foil arm. This is a problem which might lead to deterioration of the seal and possible sealing failure.

Asymmetrical Clamp Design: The asymmetrical clamp design was the final iteration of the symmetrical clamp design. The asymmetrical design solved the issues seen in the symmetrical clamp during angle of attack adjustment periods. This was selected for application in our final design.

Collet Design: The collet design would fix around the outer edge of the bar. A threaded piece would tighten over the fingers, clamping the bar inside the collet. This design had potential for easy adjustment and low slip. Our designs drawbacks included a complicated assembly and high estimated cost.

Angle of Attack Measurement

Design 1 - The first design incorporated a protractor which would be fixed to the support structure and a reading hand which would be rigidly attached to the foil arm. As the hydrofoil arm would rotate, the reading hand would indicate the angle at which the hydrofoil was at.

Design 2 - The second design involved a set of gears which would be welded to the foil arm and would work in conjuncture with a spindle set up. Angle of attach would be adjusted through rotating the spindle, each rotation would change the angle of attack by a set degree. The support structure for this would require multiple pieces to be machined and the overall design will be expensive to manufacture. The accuracy of the angle of attack measurements were expected to be acceptable.

Design 3 - The third design involved a set of key ways which would set to a particular angle of attack for each key. This would guarantee repeatability and precision but would require many parts, increasing the predicted total cost.

Design 4 - The last design involved a digital level to read in angles of attack. The foil arm would have a handle attached on which the digital level would rest and would rotate in accordance with the hydrofoil. The smart tool level we looked at for application has an accuracy of +/- .1 degree of accuracy. The digital level design benefits from simplicity and ease of attack reading.

Hydrofoil Mount

Design 1 -A basic clamping foil mount exelled in versitility but with multiple pieces would be more expensive to manufacture.

Design 2 -The top bolted foil mount incorperated bolts which would hold the hydrofoil in place through the top of the foil clamping section. This designed had less parts to manufacture but was not as versitile as clamp foil mount.

Design 3 -The back bolted foil mount had bolts which would go through the back face of the mount and pull the hydrofoil clamping section ridgedly against the inside face. This design has the least amount of parts and should be the cheapest to manufacture.

A.2 NACA foil designations

The basic shape of a National Advisory Committee for Aeronautics (NACA) airfoil can be determined by the 4-digit sequence included in the name of the hydrofoil. The first digit represents the maximum camber in percent chord length. The second digit multiplied by ten represents the location of the maximum camber in percent chord length. The NACA0012 used to obtain force design constraints for the force balance is a standard airfoil section developed by NACA. Since both of the first two digits are zero, the hydrofoil has no camber and therefore is symmetrical. Camber of hydrofoil section is the hydrofoils deviation from being symmetrical about the chord line. Figure 36 below shows an example of a cambered hydrofoil. The last two digits represent the maximum thickness in percent chord length. The chord length that was used in this analysis was 80 mm which was originally assumed to be the chord length of the majority of the hydrofoils used in this tunnel. With this chord length the maximum thickness of the hydrofoil is 9.6 mm thick and the span was chosen to be 152.4 mm because that is the inside width of the high speed water tunnel's test section. Figure 37 below shows an example of a symmetrical hydrofoil with general dimensions labeled.

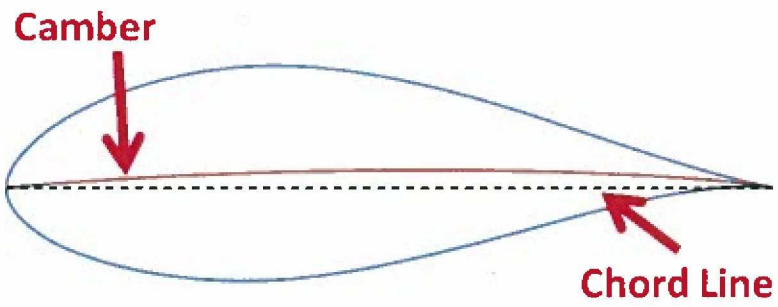

Figure 36: Example of a cambered hydrofoil section

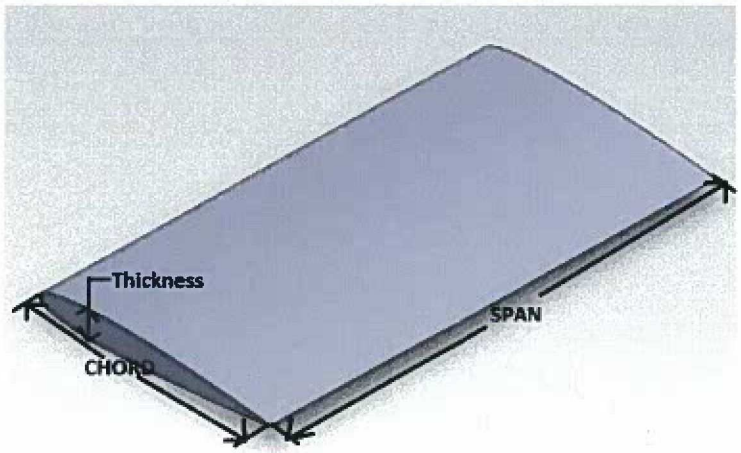

Figure 37: General dimensioning of a hydrofoil section

A.3 Additional Images

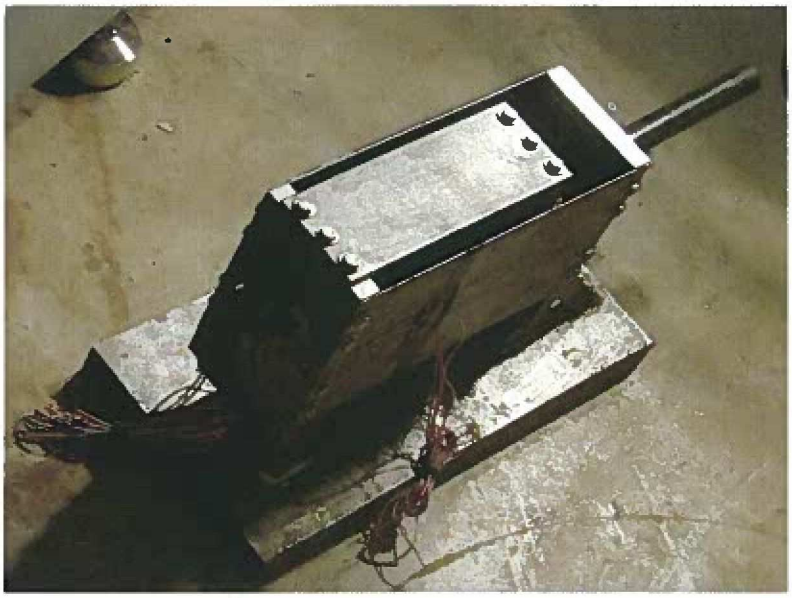

Figure 38 - Prototype force balance used for proof of concept

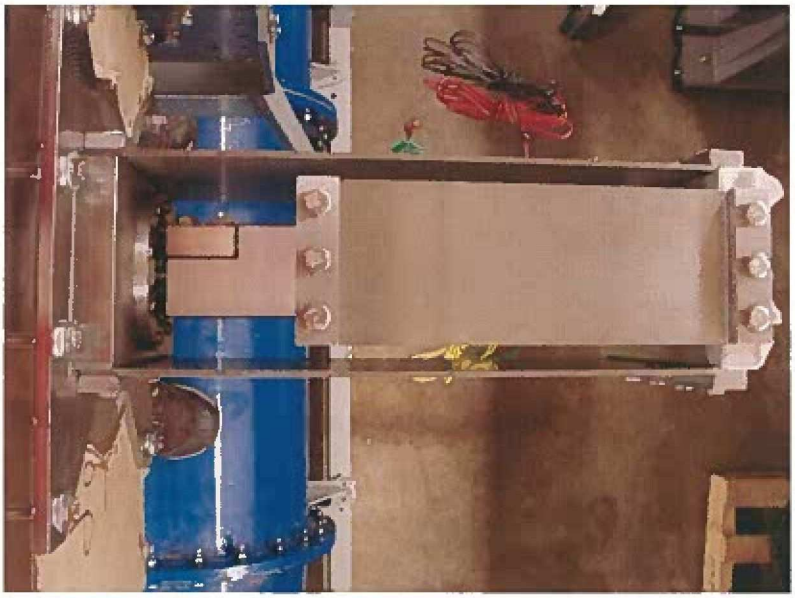

Figure 39 - Top view of final force balance connected to tunnel

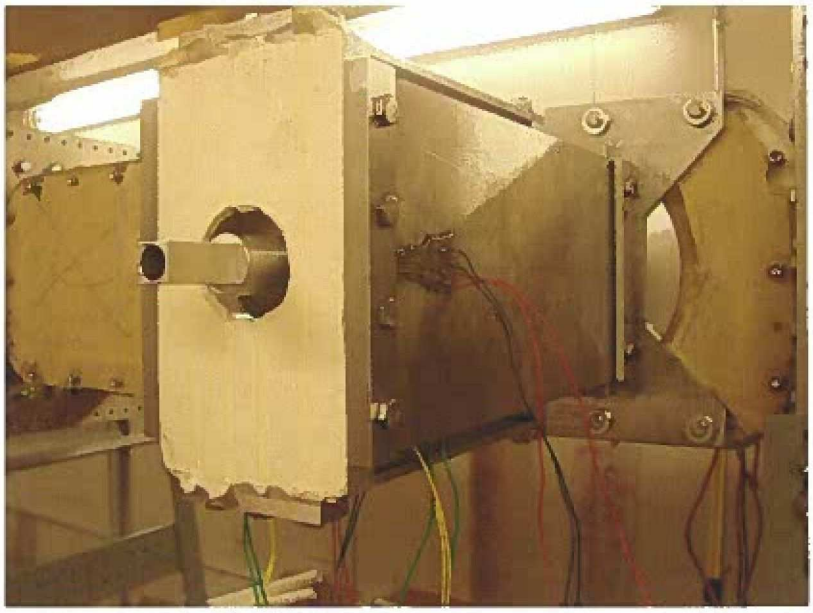

Figure 40 - Front view of installed final force balance

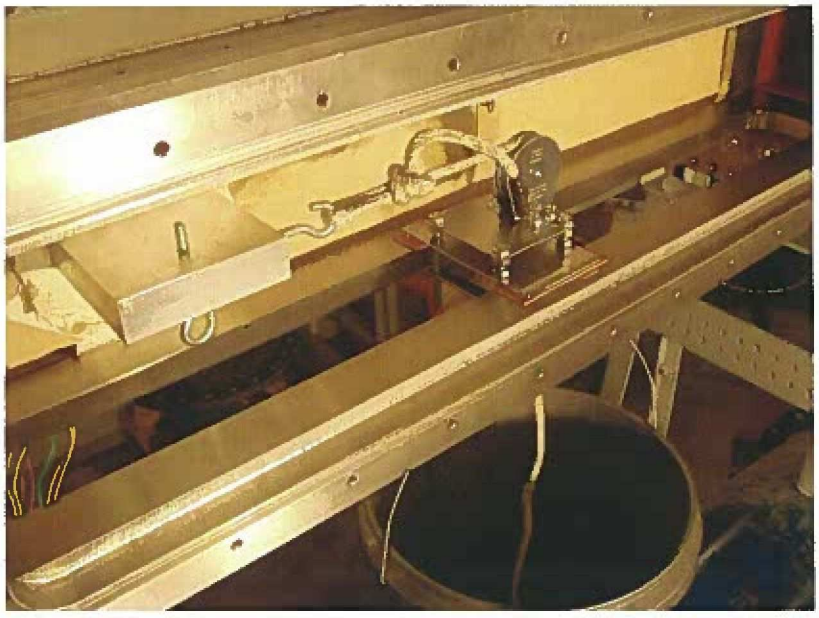

Figure 41 - Force balance calibration